An Experiment to Investigate the Stability of Evaporating Films in Micro-Gravity

Juan Carlos Gonzalez-Pons

A thesis

submitted in partial fulfillment of the

requirements for the degree of

Master of Science in Aeronautics and Astronautics

University of Washington

2013

Committee:

James C Hermanson

Dana Dabiri

Program Authorized to Offer Degree:

Aeronautics and Astronautics

Table of Contents

List of Figures

List of Tables

Introduction

Several experiments and numerical simulations [1-10] have been conducted to research the behavior of evaporating films under normal-gravity conditions. These experiments have shed light into the heat transfer properties and evaporation rate of evaporating films and terrestrial engineering applications have greatly benefited from lab experiments in which gravity conditions are standard 1-g. However, relatively little is known about the behavior of evaporating films under reduced-gravity conditions. A better understanding of this problem will positively impact the development of many of the space applications which rely upon the principle of phase change for example, for enhanced heat transfer efficiency and more effective heat rejection devices. The scope of the present research is to build an experimental apparatus which can be mounted aboard NASA's reduced gravity aircraft in order to simulate zero-g conditions. Future applications to benefit from this investigation may include spacecraft thermal control applications, such as heat pipes, capillary pumped loops and loop heat pipes. Detailed understanding of evaporation phenomena under reduced-gravity conditions is also important to the development of closed-loop life support systems necessary for long-duration human space exploration such as waste water reuse and recovery.

Theoretical Background

The convective behavior of liquid films has been greatly studied for over a century. The first experiments were developed by Bénard [1]. Rayleigh expanded on the Bénard's experiments and performed some improved theoretical analysis of the phenomena [2]. Since then, our understanding of the phenomena has increased considerably. Nevertheless, there is still no complete theory on the exact behavior of convective films. For example, there is still no comprehensive explanation of why the preferential steady pattern in many cases is the hexagonal cell. Equally, no explanation exists that can adequately explain the interaction between subcritical patterns observed at lower Rayleigh numbers when convective structures are not fully developed, generally induced by the shape of the boundary (square, circular, etc), and the super-critical cells. More research must be done in order to answer this question and

others such as the fluid behavior below critical Rayleigh and Marangoni numbers (ratios of buoyant to viscous effects and thermocapillary to viscous effects respectively) and the cause of other convective structures such as concentric rings. These are some of the questions explored by the authors of the research presented below.

The following derivation of both the Rayleigh and Marangoni instabilities follows that of Koschmieder [11]. Beginning with convective heat transfer theory, in which a thin fluid layer is heated from below and/or cooled from above, the governing equations are continuity

$$\frac{\partial \rho}{\partial t} = \nabla \cdot (\rho \mathbf{v}), \tag{1}$$

the Navier-Stokes equation

$$\rho \frac{\partial \mathbf{v}}{\partial t} = -\nabla p + \rho \mathbf{g} + \mu \nabla^2 \mathbf{v} \ , \tag{2}$$

the equation of thermal conduction ignoring viscous dissipation and assuming constant pressure

$$\frac{dT}{dt} = \alpha \nabla^2 T \ , \tag{3}$$

and an equation which relates the density changes to temperature changes linearly , commonly known as the Boussinesq approximation

$$\rho = \rho_0 (1 + \beta \Delta T), \tag{4}$$

where ρ is the density of the fluid, $\boldsymbol{g}$ the acceleration of gravity, μ the dynamic viscosity, α the thermal diffusivity, and β the volumetric expansion coefficient. The Boussinesq approximation for current purposes means that the material property changes are negligible, provided a small temperature variation, and density changes due to temperature only influence the vertical direction. The equations for a fluid film at rest are

$$\mathbf{v} = 0, \quad \frac{d^2 T}{dz^2} = 0, \quad \frac{dp}{dz} = \rho_0 g \left[1 - \beta (T(z) - T_0)\right], \tag{5}$$

where ρ_0 is the density of the fluid at the initial temperature T_0, and **v**, T and p are the actual fluid velocity, temperature and pressure respectively. With the use of the following non-dimensional parameters

$$x_i' = \frac{x_i}{d}, \quad t' = \frac{\alpha t}{d^2}, \quad u' = \frac{du}{\alpha},$$
$$\theta' = \frac{\beta g d^3 \theta}{\nu\alpha}, \quad p' = \frac{p d^2}{\rho_0 \alpha^2}, \tag{6}$$

where u is a horizontal velocity component, θ is an infinitesimal deviation in the vertical linear temperature distribution, ν is the kinematic viscosity and d is the depth of the fluid, the governing equations become

$$\nabla \cdot \mathbf{v} = 0 \tag{7}$$

$$\frac{\partial \mathbf{v}}{\partial t} = -\nabla p + Pr\ \theta \mathbf{e}_z + Pr\ \nabla^2 \mathbf{v}, \tag{8}$$

$$\frac{\partial \theta}{\partial t} = \nabla^2 \theta + Ra \cdot w \tag{9}$$

where w is the vertical velocity component and $\mathbf{e}_z$ is the unit vector in the vertical direction. It should be noted that equation 8 is dimensionless form. The prime symbols after the variables were dropped for mathematical convenience. Ra is the Rayleigh number defined as

$$Ra = \frac{\beta g \Delta T d^3}{\nu\alpha}, \tag{10}$$

and Pr is the Prandtl number defined as

$$Pr = \frac{\nu}{\alpha}. \tag{11}$$

After eliminating the pressure, horizontal velocity components, and the infinitesimal deviation of normalized temperature from the originally linear vertical temperature distribution, θ, the result is the following equation, which focuses on the vertical velocity w only

$$\left[\frac{\partial}{\partial t} - \nabla^2\right]\left[\frac{1}{Pr}\frac{\partial}{\partial t} - \nabla^2\right]\nabla^2 w = Ra \cdot \nabla_2^2 w. \tag{12}$$

The boundary condition on a rigid surface is

$$\theta = 0, \quad w = \frac{\partial w}{\partial z} = 0 . \tag{13}$$

With some mathematical manipulation [4,8], and the aid of the two dimensional wave equation

$$\nabla_2^2 f(x,y) + a^2 f(x,y) = 0 , \tag{14}$$

where *a* is the wave number, equation 14 reduces to

$$\nabla^6 w = Ra \nabla^2 w . \tag{15}$$

Skipping over some details [4,8], the resulting solution for the critical Rayleigh number, *Ra*, is given by

$$Ra = \frac{(\pi^2 + a^2)^3}{a^2\{1 - 16a\pi^2 \cosh^2(a/2)/[(\pi^2 + a^2)^2(\sinh a + a)]\}} . \tag{16}$$

The result is plotted in fig 1 where the minimum determines the critical Rayleigh number, which can be thought of as the number at which Rayleigh-Bénard (*RB*) convection is guaranteed to occur, though this is an oversimplification of the problem, since it is known that there is an important sub-critical behavior, and that the linear approximation is a very crude assumption in some cases, such as in very volatile films which undergo very rapid evaporations.

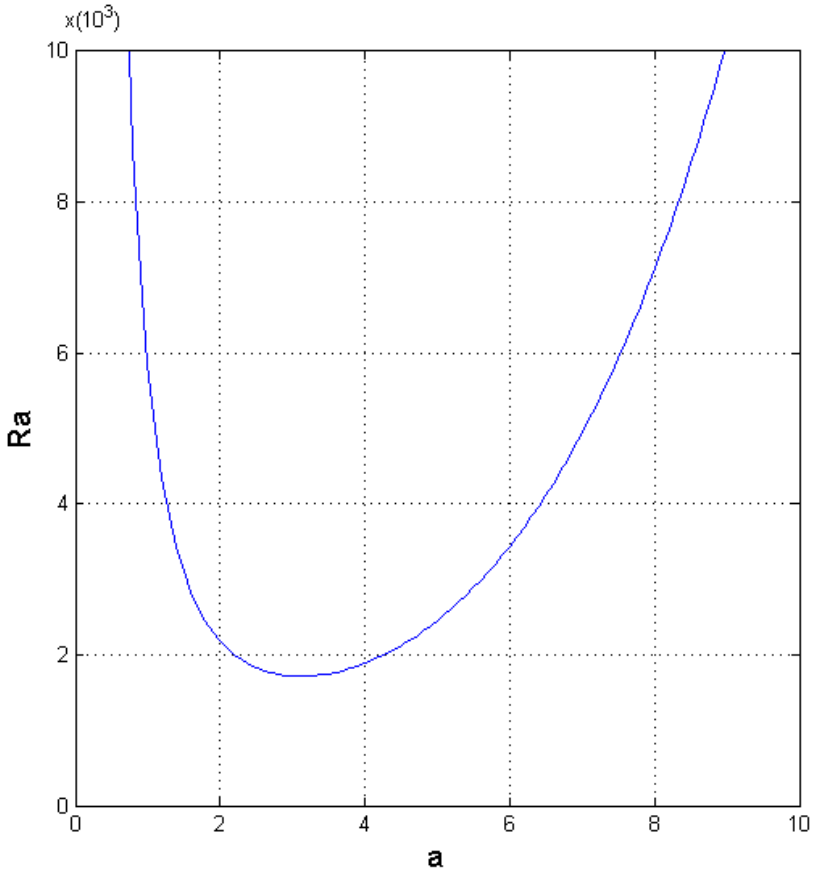

Figure 1: Neutral Rayleigh number as a function of wave number. The minimum on the curve corresponds to the critical Rayleigh number for non-evaporating films with a flat wall at the upper boundary. The stable region lies below the curve where as the unstable lies above. Ra_c = 1707 and a_c =3.117 for this case.

For the case of Marangoni-Bénard (*MB*) convection, which is surface-tension driven, a similar procedure using linear theory can be followed in order to obtain the critical Marangoni number at which the flow instability is guaranteed to take place. The Marangoni number *Ma* can be defined as

$$Ma = \frac{\partial \mathrm{S}}{\partial T}\frac{\Delta T d}{\rho \nu \alpha}, \tag{17}$$

where *S* is the surface tension. The corresponding solution for the critical Marangoni number is

$$Ma = \frac{8a(a\cosh a + Bi\cdot\sinh a)(a - \sinh a\cosh a)}{a^3\cosh a - \sinh^3 a}, \tag{18}$$

where $Bi = hd/k$ is the Biot number, *h* being the heat transfer coefficient of the film. Figure 2 shows the neutral stability plots for different Biot numbers. This solution was first obtained and plotted by Pearson

[4] and it is only appropriate when considering a film on a thermally conductive wall. A slightly different solution is needed for the insulating wall case. It was Nield [5] who combined buoyancy and surface tension into a model that represented both *RB* and *MB* convective effects. It should also be noted that since the *RB* convection scales with the cube of film thickness *d* while *MB* convection scales linearly with *d*, *RB* requires a smaller ΔT for thicker films, while *MB* is dominant in thinner fluid layers, when all other conditions are constant. This has been extensively validated experimentally

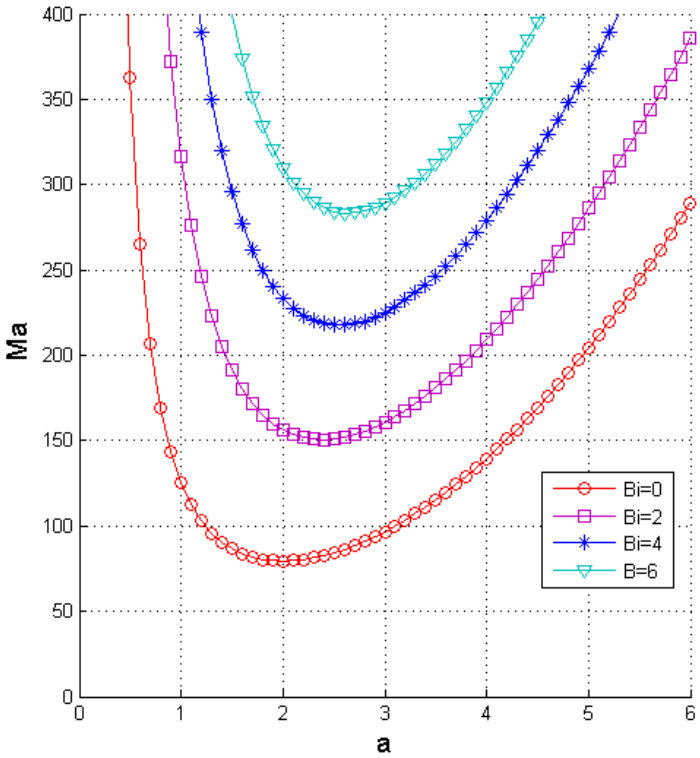

Figure 2: Neutral stability plots of Marangoni number as a function of wave number for different Biot numbers. The minima give the critical conditions for non-evaporating films, with a flat-wall at the upper boundary.

The case with evaporating films involves many destabilizing and competing effects, such as mass loss, differential surface tension, and vapor recoil, making the problem more difficult to study and model. In theory, evaporating films in microgravity should be simpler to study than those in standard gravity conditions, because all convective behavior due to buoyancy (Raleigh-Bénard) disappears with gravity, and other phenomena like thermo- capillary driven convection (Marangoni-Bénard) and vapor recoil

become the driving forces. However, the practical challenges and limitations, including the relatively high cost of conducting experiments in microgravity, add a considerably layer of complexity that should not be overlooked when considering the problem at hand. As is the case with heated films, no complete theory exists to date which can successfully explain all the phenomena associated with evaporating films either in standard or reduced gravity. The current, limited understanding of film evaporation, particularly under reduced-gravity conditions, highlights the need for zero-g experiments in order to improve the current level of understanding of the basic physics behind this scientific problem. An experimental system capable of conducting such experiments aboard the zero-g aircraft platform will be described in consequent sections.

Experiment Background

This experiment aims to describe the fundamental investigation of the mechanisms operative during film evaporation processes in reduced gravity and the corresponding impacts on the dynamic film structure and on the heat transfer. The effective removal of buoyancy in reduced gravity will drastically impact the interfacial instability of the film as it experiences mass loss, vapor recoil, and thermocapillary traction. Also of interest is the evolution of the convective structure within evaporating films in reduced gravity, where thermocapillary effects may persist but buoyant convection will be greatly diminished. The impact of all of the above on the heat transfer due to the film evaporation is also a central consideration in this work. In addition to terrestrial applications, the high heat flux associated with phase change in an important consideration in spacecraft thermal control applications.

Specific research issues to be addressed in this study include:

- What are the key changes in the stability of the evaporating film interface and the convective structure under reduced-gravity conditions, compared to normal gravity?

- What are the effects of transient thermal boundary conditions on the behavior of evaporating films, in reduced gravity, as compared to the quasi-steady evaporation that occurs for a constant level of film superheating?
- What are the corresponding implications for the evaporation rate, and for the heat transfer?

Experiment Description

The experimental procedure on board parabolic-trajectory aircraft involved a preheated film in the test chamber at the start of each low-gravity interval. Evaporation was initiated by rapidly decreasing the pressure of the saturated vapor. The goal was to keep the temperature profile within the film constant, which was achieved by supplying just enough heat via reverse thermo electric coolers (*TEC's*) so as to compensate for the temperature lost due to the evaporating liquid. Since the aircraft could provide a challenging thermal environment with ambient temperature changes of 10 ℃ or more, the test chamber was insulated in order to have the best possible temperature control. The fluid vapor also had to be kept at a very constant pressure level during the microgravity cycle. We accomplished this with the use of an expanding and contracting bladder, changes volumes accordingly matching the set pressure conditions.

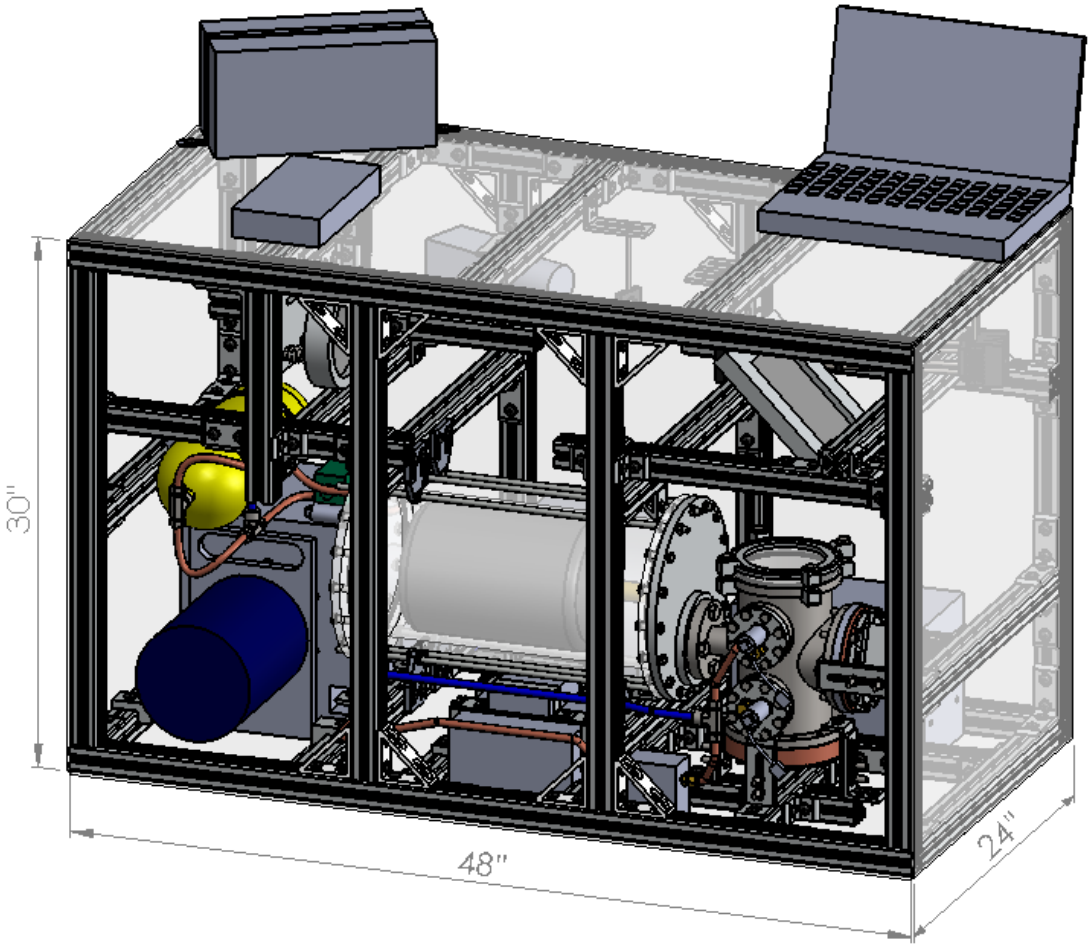

Figure 3. Experimental equipment with outlined dimensions

The candidate fluids were acetone ($(CH_3)_2CO$), dichloromethane (CH_2Cl_2), methanol (CH_3OH) and isopropanol ($(CH_3)_2CHOH$), however, the microgravity experiments were run exclusively with dichloromethane (DCM). We have used these fluids extensively in condensing and evaporating films in the laboratory. The amount of fluid needed to run the experiment is 30 ml (about 1 fluid ounce). We used already developed diagnostic techniques to determine critical temperatures, measure the dynamic film thickness, and reveal interfacial instabilities and convective structure within the evaporating films. Temperature measurements of the heated wall surface and the saturated vapor were performed using standard thermistors. An ultrasonic ranging technique developed by Kimball [9] was used to determine the thickness of evaporating fluid layers as a function of time and spatial location. This system is a

modified pulse/echo ranging system where an acoustic wave travels through the media (wall and liquid) and reflects at the interfaces. The echo return is then captured by the same transducer. By knowing the time it took for the signal to travel through the media, and knowing the speed of sound, the thickness of the film can be inferred. More details regarding this system will be given in consequent sections. The thermal patterns in the evaporating liquid will be revealed by shadowgraph or schlieren imaging, which can simply be performed using the polished metal surface as a mirror in a double-pass system.

The establishment of the evaporation flow patterns will require time scales of at least 15 seconds. The 15-20 seconds of reduced gravity available on board parabolic-trajectory aircraft will therefore allow examination of the transient behavior associated with the onset of film evaporation, and provide some insight into the subsequent quasi-steady state evaporation condition.

Equipment Description

The core of the experiment consists of a closed test cell to allow for the evaporation of a non-draining film. The test surface is circular and around 10 cm in diameter. This test surface size is sufficient to capture the most unstable wavelength for common fluids down to a gravity level of 0.01 g. The evaporation surface is heated by thermoelectric heaters. A polished copper block ensures rapid and uniform transmission of heat from the evaporating surface. An expansion chamber attached to the test cell will keep the system pressure constant to allow for a controlled rate of evaporation. Volumetric expansion will be minimized by the use of a second copper surface, from which heat will be extracted by thermoelectric coolers to condense vapor at a rate comparable to that at which it is produced by evaporation. A heated optical port will be situated directly opposite the evaporating surface. The platform was designed to carry most essential experimental hardware, including all associated plumbing, heating units and controllers, diagnostic instrumentation, and data acquisition systems. This made the experiment as self-contained as possible.

The equipment can be broken into several major components and can be seen in fig 4. Note that not all equipment is labeled.

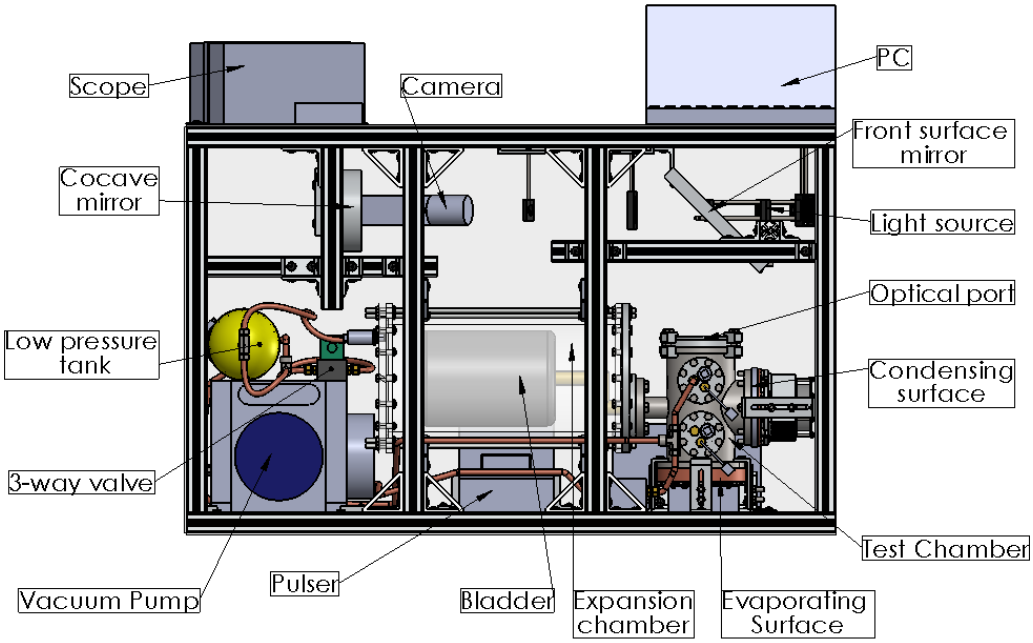

Figure 4. Major components of experimental system

Test Chamber/Expansion Chamber system

These two units work essentially as one, hence, they are best described together. The test chamber is the core of the experiment. Here is where the fluid film and part of the fluid vapor reside. The chamber is a custom-made steel chamber about 9 liters in volume. The bottom of the chamber is sealed with the evaporation surface, which is a 1 inch-thick gold-plated copper flange. The right side of the test chamber is sealed with a 1/8 inch copper flange which serves as a condensing surface to condense any excess vapor inside the system. The top of the test chamber is sealed with a ¼ inch thick Pyrex flange which serves as the optical port for the schlieren system. The test chamber is attached to the expansion chamber. The pressure of the expansion chamber is actively controlled, which lets the bladder expand or contract accordingly in order to maintain a constant fluid pressure.

Schlieren

The schlieren system is used to image the convective structure of the film. The light source consists of an 700 lm output LED, with an array of lenses and pinholes. The light is then focused on a parabolic mirror. The parabolic mirror collimates the light into a front surface mirror, which in turns reflects the light onto the film. Since the film resides on top of the gold plated copper plate, the light bounces back. The beam is eventually split with a beam-splitter and focused onto a knife edge, where half the light is blocked. The image is then captured by the camera and recorded on the computer. It should be noted that the light beam travels twice through the film, therefore the system is actually a double-pass schlieren system.

Ultrasound

The ultrasound system is used to capture the film thickness. An ultrasound signal is generated by the pulse generator. This signal is then split three-way by the multiplexer, and sent to each of the ultrasound transducers attached to the bottom of the copper plate. The signal then travels through the copper and the film, and the echo at each interface is received by the transducers. The waveform of the echo is recorded in the computer with the help of the thickness gage and a high speed scope. The system does not have real time capabilities; therefore a post-processing code is required. The code works by matching a simulated signal for which time of flight is known to the captured ultrasound data. The code runs in a combination of Matlab and FORTRAN, and has been previously discussed at length by Kimball [9]. The system has an overall precision of ±1 um and an accuracy better than 10%.

Pressure control

The pressure is controlled with an array of valves and LabVIEW code. The low pressure is achieved by an oil free scroll pump, which has already been flown. The 3-way valve controls the pressure inside the expansion chamber, allowing the bladder to expand or contract, which in turns controls the pressure inside the test chamber. If the pressure inside the expansion chamber slightly exceeds the specified pressure, the 3-way valve lets air out. The opposite happens if the pressure falls slightly below

the set pressure. A low-pressure tank is used as a buffer so that the changes in pressure are damped out. A regular 2-way solenoid valve helps control the amount of vapor inside the test chamber. The pressure is monitored by Omega® strain gages.

Temperature control

The temperature is controlled by TEC's and LabVIEW. Two sets of TEC's are used. A set of 4 TEC's heats the evaporating surface. The amount of heat needed is minimal since the only heat needed is that used to replace the heat "absorbed" by the evaporating fluid. The second set of TEC's contains 8 units, and these are used to cool the condensing surface. The temperatures of the evaporating surface and the vapor are monitored with high accuracy Omega® thermistors.

Electrical

The electrical and electronics systems consist of different power supplies, regulators and switches. Power to TEC's, fans, and valves is supplied by an array of AC-DC converters and DC-DC converters. A signal conditioning box works together with a National Instruments USB 6351® data acquisition card in order to collect temperature and pressure data. There is also a box which houses several solid state relays, used to control the operation of virtually all electronics equipment. There is also an Uninterruptible Power Supply (UPS) used as a power back up for critical equipment.

Structural Verification

In order to safely conduct the experiment aboard the reduced-gravity aircraft, several standards had to be satisfied. The first one we will discuss is the structural verification. The experimental rig had to be securely attached to the floor of the aircraft in a bolt pattern of 20 by 20 inches, and be able to withstand the following g-loadings as shown in fig 5. The frame material of choice was 80-20® Aluminum beams and brackets. We then determined the rack's maximum allowable turning moment which depends on the location of the c.g of the attached equipment. The limit is mostly bounded by the

strength of the fasteners, particularly the brackets, since the screws and beams fail at higher loads than the brackets themselves.

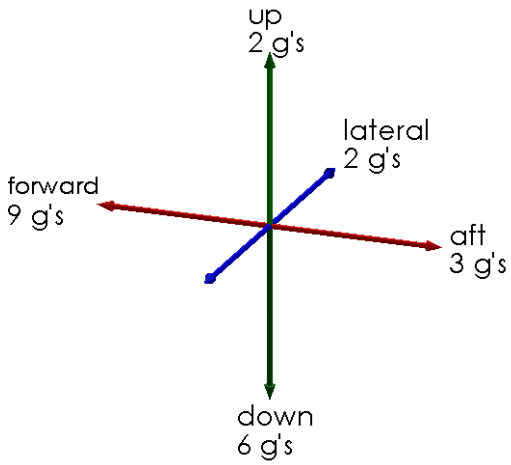

Figure 5. Load resistance and orientation which will be followed for consequent frame representations inside the aircraft.

The structural analysis will be broken into the following items:

1. The weight and c.g of the entire top and sides of the rig, both frame and equipment, which is attached to the bottom through the vertical beams. This assures that the joints along the bottom can withstand the loads generated by the top of the experiment.

2. The weight of the components attached to the top and sides of the frame. This assumes that the load is uniformly distributed by all joints, which is a very good approximation given that the beams are heavily interconnected. The moment obtained will be compared with the total maximum allowable moment of all joints on the top and side. This basically assures that the all horizontal beams can support the loads induced by the equipment. The moment arm in this case is half the distance from the front side to the back side.
3. The weight and c.g. that equipment which is attached directly to the bottom section (rather than through the vertical beam joints) and the loads they produce on the frame.

4. Structural integrity of the brackets holding the parts themselves, such as the chamber system, concave mirror etc.
5. Analysis of the loads by applied by the frame and equipment on the bottom aluminum plate.
6. Load of the entire system on the floor of the aircraft.

In this report we will only include items 1 and 2 for the case 9 g's in the forward direction. All other cases, including the calculations, will be included in appendices.

The analysis was done by following the basic static principles. Figure 6 shows the basic set up of the problem at hand for the particular case of the vertical beam loads along the bottom section. A load is applied at the top of the frame, resulting in reaction forces along the bottom junctions.

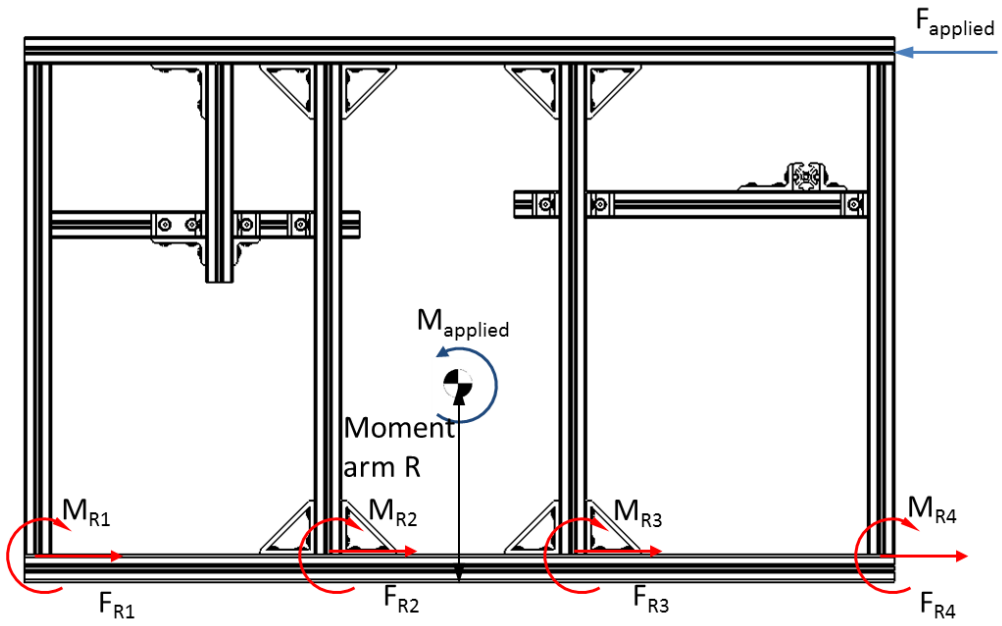

Figure 6. Applied load and reacting forces for the particular case of a forward load and reacting forces along the bottom section.

Setting up the equations we have

$$F_{applied} - \Sigma F_{R(1-8)} = 0,$$

where

$$F_{applied} = mass\ of\ attached\ equipment \times 9,$$

and

$$M_{applied} - \Sigma M_{R(1-8)} = 0,$$

where

$$M_{applied} = mass\ of\ attached\ equipment \times R\ \times 9.$$

The reason the number of reacting forces was doubled is due to the figure only showing the front face of the rig where we have 4 junctions. The back face contributes with other 4 junctions as well. This has to be accounted for when calculating the total force the junctions can withstand.

We assumed that the center of mass was located some distance directly above the geometric center of the frame bottom. What this implies is that the loads are equally distributed by the joints. This allowed carrying out the structural analysis regardless of the fact that the system is statically indeterminate. In reality, the equal loads assumption is reasonable. If the center of gravity of the equipment exerting a load on the bottom were projected down onto the base of the frame, it would fall within 1 inch of the geometrical center of the frame.

Items, 1 through 6 were done in a similar fashion. The first step was to calculate the value of the applied load (force and moment). Those values come from knowing the weight and c.g. of each element attached to the rig. The weight and c.g. table includes all the components attached to the rack (that are known at this time), is shown in Table 1. Loads and weights are calculated at 1 g. The weight and c.g table is divided into two parts, basically following items 1 and 2. It should also be pointed out that the bottom and top of the frame are symmetric along the forward-line. Hence, once the forward 9 g's loading is satisfied, the 3 g's of loading in the aft direction is assumed to be satisfied as well. Note that as this table applies to vertical beam junctions along the bottom, and equipment attached to the sides and top, all equipment which attached directly to the bottom section does not contribute to the turning moment of either of the above mentioned items, hence the turning moment in the table is listed as zero.

Table 1. Weight, c.g. and turning moment of attached equipment.

Film evaportation rig					
Weight and cg table					
	item	weight confirmation	weight (lbs)	c.g. (in)	turning moment (lb-in)
Experiment core	Test chamber/expansion chamber system	calculated	51	8.5	433.5
Schlieren	LED and lens system	measured	1.5	24	36
	Concave miror system	measured	6.5	23.5	152.75
	Front surface mirror	measured	5	24	120
	Beam splitter	measured	0.5	24.5	12.25
	Kinfe edge	measured	0.3	24.5	7.35
	Camera	measured	2	24	48
Ultrasound	Pulse generator	measured	6	2	0
	Multiplexer	measured	0.8	5	0
	Thickness gage	measured	2.1	31	65.1
	Scope		10	33	330
Vacuum equipment	Pump	measured	70	6	0
	3-way valve	measured	3	10	0
	2-way valve 1	estimated	3	1.5	0
	2-way valve 2	n/a			0
	Low pressure tank	measured	3.8	12	45.6
Electrical	UPS	estimated	8	10	0
	Relay box	estimated	1	6	6
	Current/Voltage regulator boxes	estimated	1.5	7	10.5
Data acquisition	Computer	spec sheet	5.5	31	170.5
	USB 6351	measured	2.5	3	0
Inner beams	Transverse totals (1515-LS)	calculated	11	14.5	159.5
	Longitudinal totals (1515-S)	calculated	9.14	21	191.94
	Vertical totals (1515)	calculated	2.47	23.5	58.045
Plexy covers	Top	measured	9	31	279
	Front and back	measured	22	15	330
	Left and Right	measured	11	15	165
			weight of top and sides		turning moment on top and sides
			248.61		2621.035

Table 1 (continued). Weight, c.g. and turning moment of attached equipment.

Frame	Top transverse beams		11.8	29	342.2
	Front and back sides		25	27.2	680
	Right and left beams		4.7	12	56.4
	Bottom beams		24	0	0
	Bottom plate		28	0	0
	Brackets, bolt and fasteners (top only)	Solidworks	23	16.5	379.5
	Brackets, bolt and fasteners (bottom)	Solidworks	15	0	0
			frame weight	frame c.g.	frame turning moment
			116.5	12.52	1458.1
			weight of rig		**turning moment on bottom**
			404.11		**4079.14**

Before identifying failure limits, we will introduce the basic nomenclature to be followed in order to make the structural analysis easier to navigate. The rest of the figures will be attached in corresponding appendices. Table 2 shows a picture of one of the joining brackets used in the rig, with a graphical representation of the force, or moment applied. Also included are the part number and a labeling system used when referencing such part undergoing the given load. This nomenclature will be used extensively later in the tables detailing the maximum load limits the frame can experience, allowing us to efficiently reference those values.

Table 2. Sample nomenclature used when referencinc bracket limits.

Part and mode: 4301 Shear Force 1 Nomenclature: 4301s1 Failure point: 1200 lbs (Pull Test) Failure cause: Sliding of the T-nut-screw-bracket system	Part and mode: 4301 Moment 1 Nomenclature: 4301m1 Failure point: 500 in- lbs (Pull test corroborated by ANSYS) Failure cause: Plastic deformation of the bracket
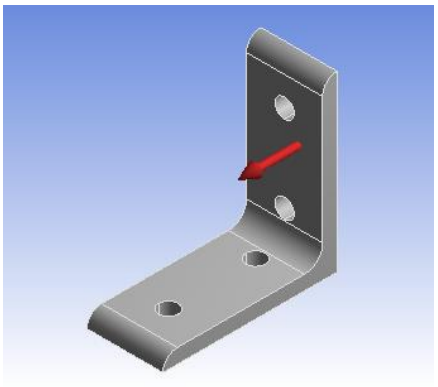	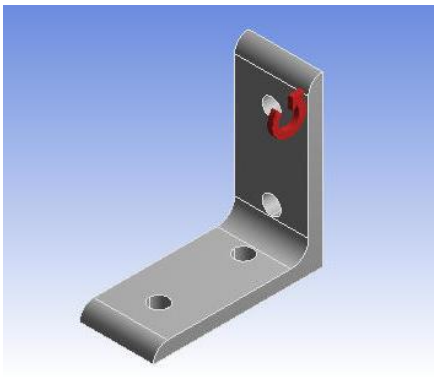

It is also important to understand the system used to label the junctions themselves. The junctions can be held together by one or several parts, which could also be different. So each junction will have a maximum load which it can sustain. Figure 7 shows the nomenclature used to label the junctions of the vertical beams along the bottom of the frame. The frame will be mounted in the plane as oriented as depicted back in fig 5.

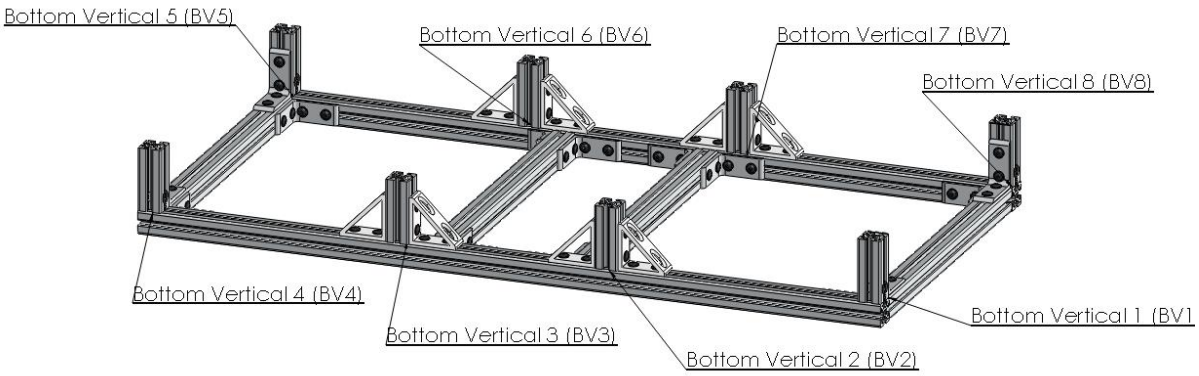

Figure 7. Nomenclature used to lable junctions of vertical beams along the bottom of the frame.

We then need to identify the failure mode (shearing, plastic deformation etc…), and most importantly, the failure limit. As can be guessed from table 3, for most applications the failing element within the junction turned out to be the joint bracket, failing at lower stresses than the shearing or stripping of the screws, or the bending and buckling of the beams. It should be pointed out that the maximum allowable load for each bracket was not readily available. 80-20 did provide some of those data, but they were extremely generic, and in some cases, did not match experimental observations. The missing data were obtained experimentally, using FEA (done in ANSYS or SolidWorks), from MIL-HDBK5, or from the pull tests as shown above. We generally assumed whichever method gave us the lowest limit, hence ending up with the most conservatives of estimates. Table 3 shows the failure limit of the bottom junctions.

Table 3. Maximum load values for brackets and joints along bottom.

Vertical beams bottom junctions tolerance along the forward-aft line						
Junction		Joining Method	Shear failure mode	Max allowable shear force (lbs)	Moment failure mode	Max alloawable moment (in-lbs)
BV1		3095	3095s1	1200	3095m1	7200
		1 * 4336	4336s2	5460	4336m3	1200
BV2		1 * 4336	4336s1	1200	4336m1	4000
		1 * 4336	4336s1	1200	4336m2	3700
BV3		Same as BV2	(see above)	2400	(see above)	7700
BV4		Same as BV1	(see above)	6660	(see above)	8400
BV5		Same as BV1	(see above)	6660	(see above)	8400
BV6		Same as BV2	(see above)	2400	(see above)	7700
BV7		Same as BV2	(see above)	2400	(see above)	7700
BV8		Same as BV1	(see above)	6660	(see above)	8400
Total				**36240**		**64400**

With the applied load values and the maximum allowable load at the junctions, we can then calculate resulting safety factor using the following equations:

$$\frac{\Sigma F_R}{F_{applied}} \geq 2$$

and

$$\frac{\Sigma M_R}{M_{applied}} \geq 2.$$

Table 4 shows the resulting safety factors for the vertical beam junctions along the bottom.

Table 4. Safety factors for vertical beam junctions along bottom.

Bottom junctions 9 g's forward condition						
Bottom junctions limit in force (lbs)		36240		Bottom junction moment limit (lbs)		64400
Force under 9 g's forward loading (lbs)		2611		Moment under 9 g's forward loading (in-lbs)		35227
Safety factor (Force)		14		Safety factor (Moment)		2

We followed the same process to analyze the top and side sections of the frame. The weight of the equipment attached to the top and sides is already in table 1. The nomenclature we will use is based on fig 8.

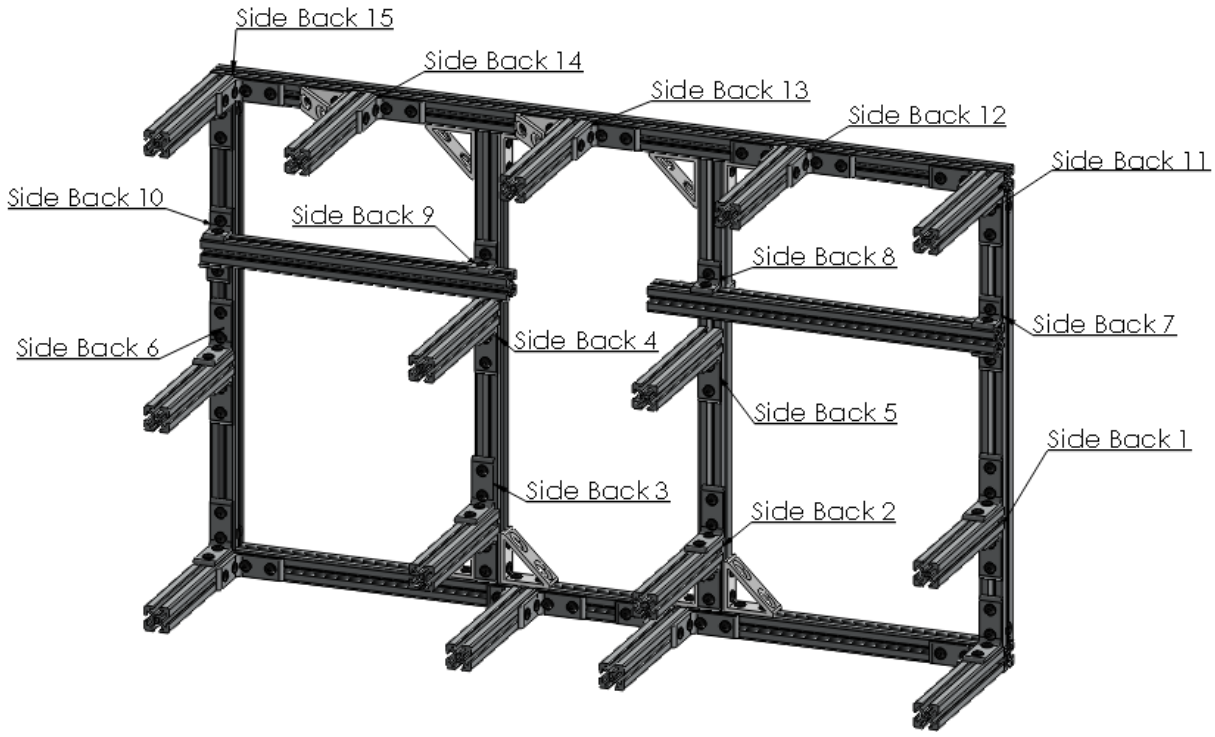

Figure 8. Side junctions lableing system.

The maximum allowable limits are shown in table 5.

Table 5. Tolerances of top and sides junctions along the forward aft line

Top and sides along the forward aft line						
Junction		Brackets	Shear failure mode	Max allowable shear force (lbs)	Moment failure mode	Max alloawable moment (in-lbs)
Side Back 1		2 * 4301	4301s2	10800	4301m3	2000
Side Back 2		Same as SB1	4301s2	10800	4301m3	2000
Side Back 3		Same as SB1	4301s2	10800	4301m4	2000
Side Back 4		1 * 4301	4301s2	5400	4301m3	1000
Side Back 5		Same as SB 4	4301s2	5400	4301m3	1000
Side Back 6		Same as SB1	4301s2	10800	4301m3	2000
Side Back 7		2 * 4302	4302s1	1200	n/a	
Side Back 8		1 * 4302	4302s1	600	n/a	
		2 * 4302	4302s1	1200	n/a	
Side Back 9		1 * 4302	4302s1	600	n/a	
		1 * 4302	4302s1	600	n/a	
Side Back 10		2 * 4302	4302s1	1200	n/a	
Side Back 11		1 * 4301	4301s2	5400	4301m3	1000
		1 * 4301	4301s1	600	4301m1	500
Side Back 12		1 * 4301	4301s1	600	4301m1	500
		1 * 4301	4301s1	600	4301m2	500
Side Back 13		1 * 4301	4301s1	600	4301m2	500
		1 * 4336	4336s1	1200	4336m1	4000
Side Back 14		Same as SB 13	4301s1	600	4301m2	500
			4336s1	1200	4336m1	4000
Side Back 15		Same as SB 11	4301s2	5400	4301m3	1000
			4301s1	600	4301m1	500
Total for SB				76200		23000
		Side Front equal to Side Back				
Total for sides				**152400**		**46000**

The safety factor calculation is shown in the table 6.

Table 6. Safety factors for top and sides subject to the 9 g's forward loading condition.

Top and sides							
Limit in force (lbs)		152400		Top and sides moment limit (in-lbs)			64400
Force under 9 g's forward loading (lbs)		1197		Moment under 9 g's forward loading (in-lbs)			13766
Safety factor (Force)		127		Safety factor (Moment)			5

Electrical Analysis

The electrical load of the entire rig had to be specified calculated and submitted to NASA prior to the flight, as well with electrical schematics. The experiment required two 120 V, 60 Hz and two 28 VDC, 15 A aircraft feeds. The electrical schematic and load tables are shown below.

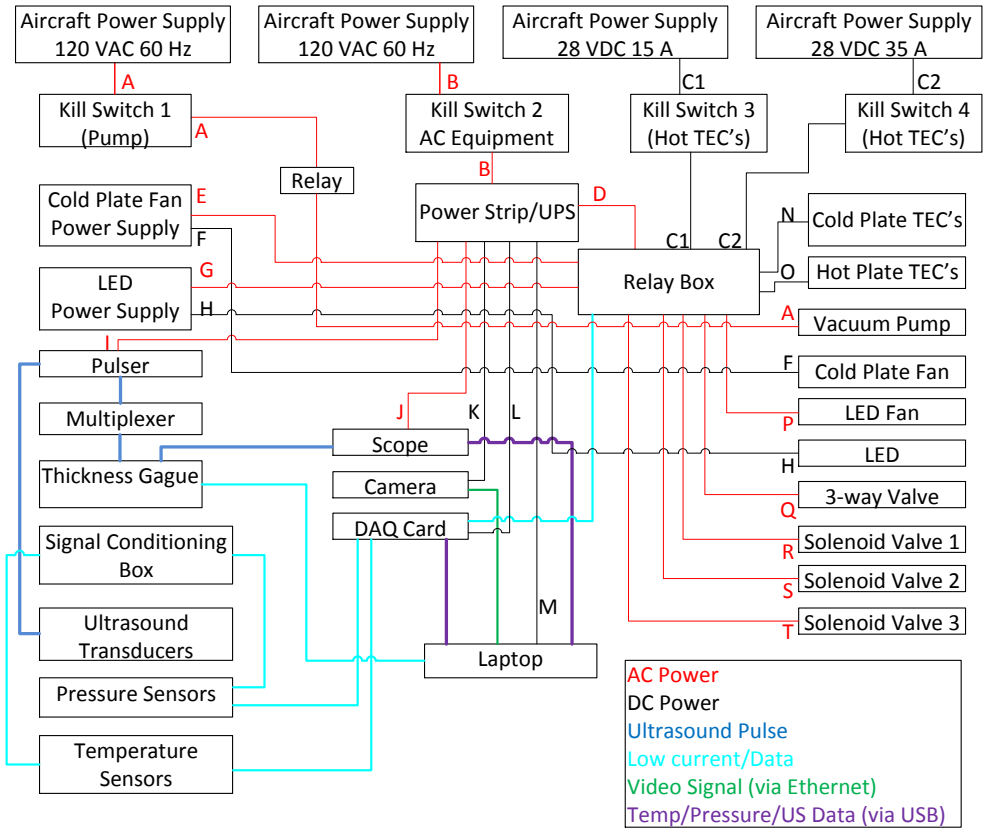

Figure 9. Electrical schematic.

Table 7. List of all electrical equipment in the experiment

Designation	Gauge	Current	Description
A	12	17.5 A	Cord through killswitch 1, pump relay and vacuum pump
B	14	5.62 A	Power Strip with 15 Amp integrated breaker
C1	14	12 A	Aircraft DC current 28 VDC, 15 A (for cooling TEC's)
C2	14	24 A	Aircraft DC current 28 VDC, 35 A (for heating TEC's)
D	14	1.77 A	Relay Switch Box (Assembled in house with appropriates solid state relays for each line)
E	18	0.7 A	Cold Plate Fan Power Supply (pending)
F	24*	1 A	Cold plate fan
G	18	0.3 A	LED Power Supply (pending)
H	24	1 A	LED Luxeon Altilon LAFL-C4-0700
I	18	0.2 A	Pulse Generator Olympus 5072PR
J	18*	1 A	Scope Agilent Technologies DSO5054A
K	22	0.35 A	Camera Panasonic WV-SP302
L	18*	0.8 A	Data acquisition card NI USB-6351
M	18*	1.5 A	Laptop PC HP ProBook 4525s
N	20*	16 A	Cold plate TEC's

			V-Infinity CP60440
O	20*	8 A	Hot plate TEC's V-Infinity CP60440
P	24*	0.2 A	LED fan Sunon MA1062-HVL
Q	16*	0.12 A	3-way valve Numatics 152SA400K
R	16*	0.15 A	Solenoid valve 1 ASCO Red Hat 8210G26T
S	16*	0.15 A	Solenoid valve 2 ASCO Red Hat 8030A67
T	16*	0.15 A	Solenoid valve 3 ASCO Red Hat 8030A67

* - UL Listed Power cord supplied by manufacturer of equipment.

Table 8. Load table for vacuum pump circuit.

Power Source Details		Load Analysis	
Name: Voltage: Wire Gauge:	Vacuum pump 115 VAC, 60 Hz 12	Vacuum pump	17.5 A
Max total current	41 amps	Total current draw	17.5 A

Table 9. Load table for power strip.

Power Source Details		Load Analysis	
Name:	Power strip/UPS	Cold plate fan power supply	0.7 A
Voltage:	115 VAC, 60 Hz	LED power supply	0.3 A
Wire Gauge:	14	Pulser	0.2 A
		Signal conditioning box	
		Scope (through UPS)	1 A
		Camera (through UPS)	0.35 A
		DAQ card (through UPS)	0.8 A
		Laptop PC	1.5 A
		LED fan (through relay box)	0.2 A
		3-way valve (through relay box)	0.12 A
		Solenoid valve 1 (through relay box)	0.15 A
		Solenoid valve 2 (through relay box)	0.15 A
		Solenoid valve 2 (through relay box)	0.15 A
Max total current	15 amps	Total current draw	5.62 A

Table 10. Load table for 28 V DC, 15 A input circuit.

Power Source Details		Load Analysis	
Name:	DC Input	Cold Plate TEC's	12 A
Voltage:	28 VDC		
Wire Gauge:	14		
Max total current	32 amps	Total current draw	12 A

Table 11 . Load table for 28 V DC, 35 A input circuit.

Power Source Details		Load Analysis	
Name:	DC Input	Hot Plate TEC's	24 A
Voltage:	28 VDC		
Wire Gauge:	14		
Max total current	32 amps	Total current draw	24A

In order to ensure that no researcher was at risk of electrical shock, virtually all of the AC equipment was connected with a 3-prong connector to the power strip/UPS, or to the aircraft directly as is the case with the pump. Equipment which did not have a 3-prong connector was grounded through the frame by connecting a metal portion of the frame to the frame. This applied to all solenoid valves (including the 3-way valve). The only exception was the LED fan. This fan had only two wires coming out of it, and every exposed surface is made of plastic.

Emergency Shut-Down Procedures

An emergency shut-down procedure was established as well. We routed all the equipment through three emergency kill switches in total: one for the vacuum pump line only, one for the DC input line, and another integrated into the power strip. All three kill switches were placed in close proximity so that all could be easily accessible in case of an emergency shutdown. Power shutdown using these switches severs all power and the system falls to safe mode with no harm to operator or apparatus.

Pressure Vessel / System

Another important element to consider was the pressurization of the test chamber, expansion chamber and tanks. Even though they were always under sub-atmospheric conditions, meaning, they were never pressurized, under some extreme conditions (i.e. total cabin pressure loss in the aircraft at the highest possible altitude it can reach) it was theoretically possible to end up with positive pressure in

some of the components. A thorough study of all components was done in house, including hydro-dynamic tests and worst-case scenario calculations.

The experiment's pressure system layout is shown in fig10 and a schematic of the same system is shown in fig 11.

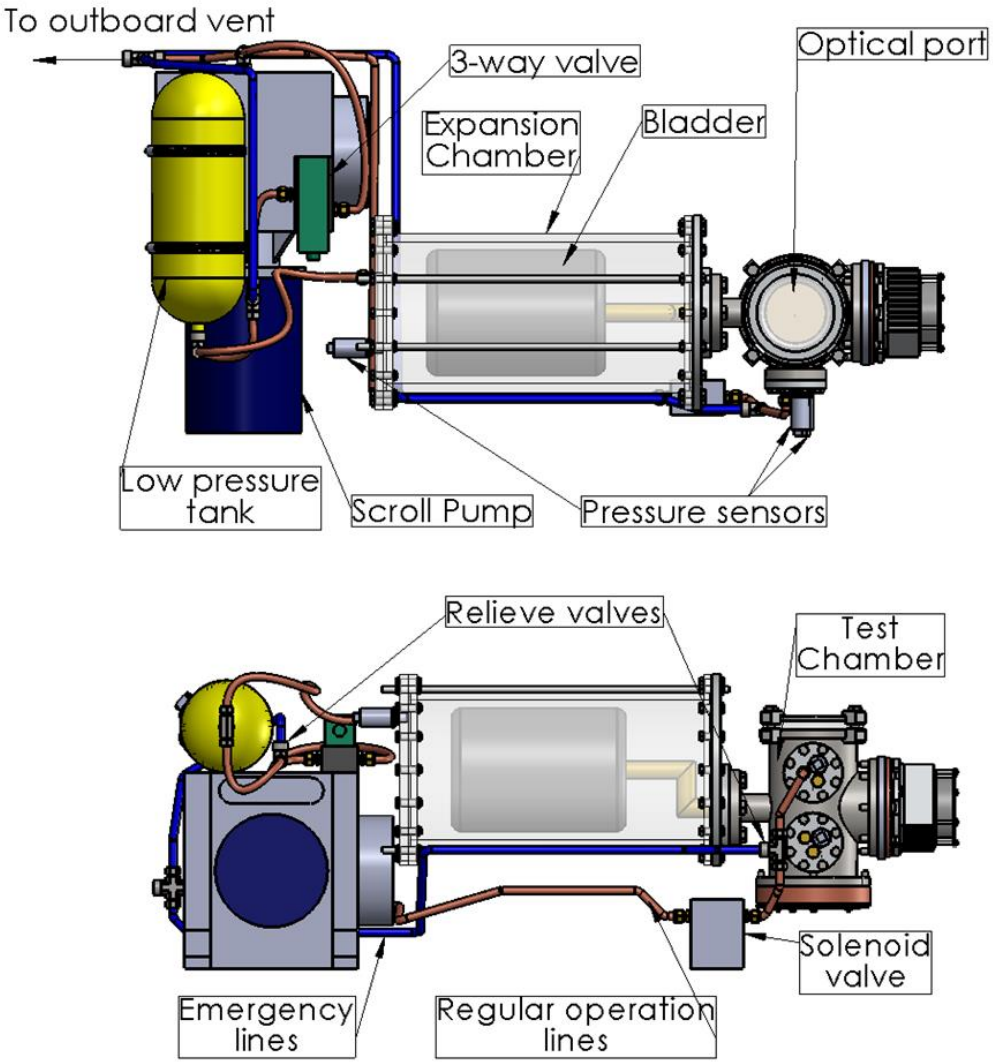

Figure 10. Top view (top) and front view (bottom) of the P/V system. (Solenoid valves 2 and 3 not included in drawing)

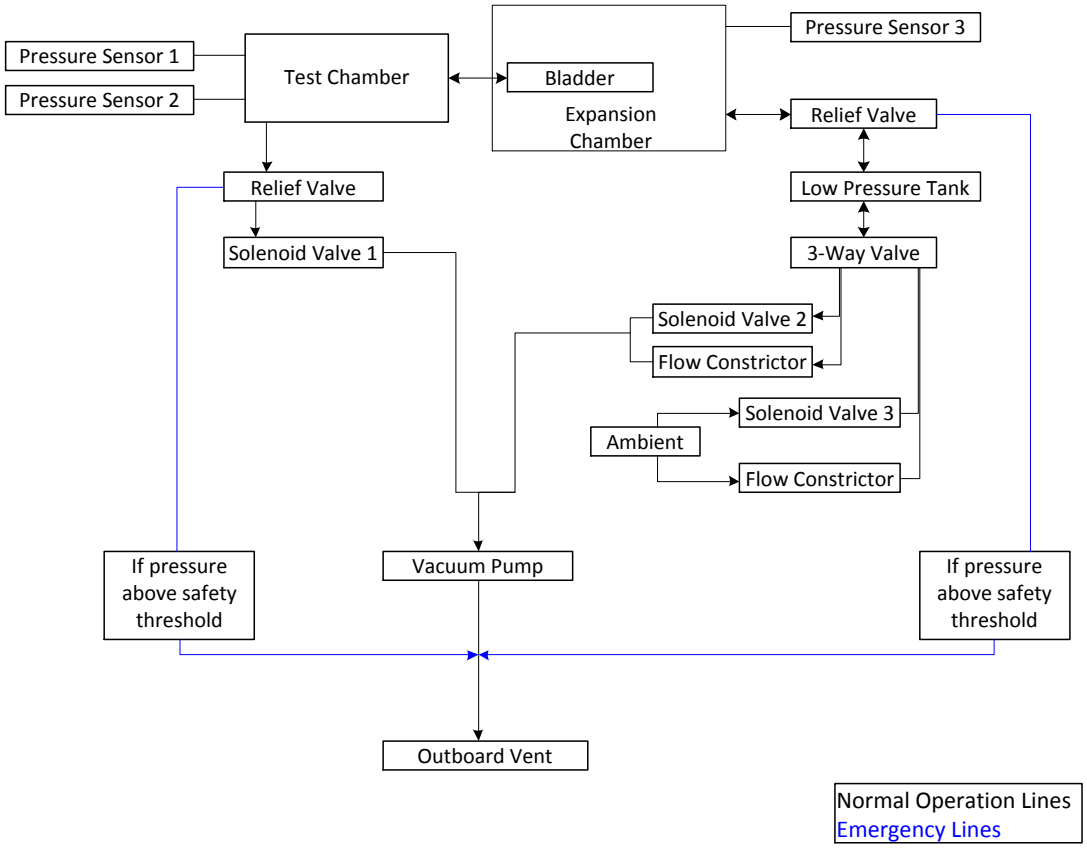

Figure 11. Schematic of P/V system.

As stated above, the system normally operates under vacuum condition. The only possibility for the system to become pressurized would occur in the event of a loss of cabin pressure. Even in these scenarios, the pressures will remain extremely low. There are two possible situations regarding the system's response to an over pressurization. Both of these will be studied below. We will also attach known MAWP for the experiment components.

Both situations assume the worst possible case scenario, that is, all of the working fluid is in vapor form, and the aircraft, at its highest possible altitude, experiences a total cabin depressurization.

Situation 1:

Under the above mentioned circumstances, the fluid occupies the test chamber and expansion chamber volumes only. This assumes that the bladder will not rupture while it expands to fill the volume of the expansion chamber. This event is somewhat unlikely since in reality, the bladder will probably rip along the seams. Assuming the bladder will not rip we have:

- Highest possible amount of vapor: 0.52 moles (for the case of Methanol)
- Highest temperature reached by vapor (this is based on the amount of heat the TEC's can pump into the system, and the value assumed is at least 3 times higher than anything reached experimentally): 100 °C.

- Volume of test chamber/expansion chamber system: < 20 liters.
- Pressure given the above conditions (assuming ideal gas conditions): 0.8 atm (11.8 psi)
- Air pressure at 40000 feet: 2.71 psi

Under such conditions the system pressure is:

$$(11.8 - 2.71) \text{ psi} = 9.09 \text{ psi}.$$

Situation 2:

Under the same premise, the bladder ruptures in this case, so the entire volume to be filled is the test chamber, expansion chamber, low pressure tank, and connecting pipes up to the 3 way valve (volume of pipes will be ignored).

- Volume of low pressure tank: 4.6 liters
- Increase of volume (compared to last case): 23 %
- Corresponding decrease in pressure leads to: 9.86 psi

Under such conditions the system pressure is:

$$9.86 - 2.71 \text{ psi} = 7.15 \text{ psi}$$

Table 12 shows the pressure rating of the vacuum system. As it can be seen the resulting pressures in the worst possible scenarios are considerably low compared to the pressure ratings of the equipment shown.

Table 12. Pressure rating of major components in P/V system.

Part	Manufacturer	Part No.	Pressure rating
Test Chamber	A&N Vacuum	Custom	55 psi (Hydrostatic test)
Optical Port ¼ by 6 in dia Pyrex plate	Chemglass	CG-1906-23	50 psi (hydrostatic test) 270 psi (numerical simulation)*
Cold plate	Built in house	n/a	55 psi (hydrostatic test)
Hot plate 6" dia by 1" thick Copper flange	Built in house	n/a	2000 psi (numerical simulation)*
Instrument ports 3.5" dia by 0.4" thick 6061 Al flanges	Built in house	n/a	55 psi (hydrostatic test)
Expansion Chamber body	Built in house	n/a	400 psi (Numerical simulation)*
Expansion chamber Plexy face 11" dia by 0.5" thick Plexyglass	Built in house	n/a	14.7 psi (tested during normal operation) 50 psi (Numerical simulation)
Expansion chamber Al face 11" dia by 0.5" thick 6061T6 Al	Built in house	n/a	300 psi (numerical simulation)*
Low pressure tank	DK Manufacturing	MK57-100	50 psi (stated by manufacturer)
Copper tubing ¼ nominal	Mueller Industries	Type L	500 psi (listed in NASA JPR1710.13E)
Flex hose tubing	Swagelok	PB-6	300 psi (stated by manufacturer)
Relief valves	Aquatrol	89A2-15	15 psi (set pressure)
Pressure sensors	Omega	PX312-015AV	30 psi (working limit)**
3-way solenoid valve	Numatics	152SA400K000030	28" Hg vacuum to 150 PSIG
2-way solenoid valve 1	Asco Red Hat	8210G26T	300 psi
2-way solenoid valve 2	Asco Red Hat	8030A67	15 psi
2-way solenoid valve 3	Asco Red Hat	8030A67	15 psi

*Numerical simulations indicate the failure point of the given part analyzed. No safety factors are included in the simulations. The safety factor for the system will be calculated below.

** The working limit of the pressure sensor was the only value provided by the manufacturer. However, it was also stated that failure of the sensor would not be catastrophic (i.e, parts becoming loose, etc). The sensor would just stop working, but all parts would be remain attached.

Some items shown in table 12 would fail at such extremely high pressure values that the failure would occur at the fasteners. Assuming that the screws would fail in tensile mode, the failure of each of the above mentioned parts would occur at the values shown in table 13.

Table 13. Tolerance values of fasteners used in the P/V system

Item	Fasteners	Tensile limit (ksi/screw)	Total (ksi)
Hot plate	12 * 5/16-24 screws	4020	48240
Cold plate	8 * 5/16-24 screws	4020	32160
Instrument ports	8 * 5/16-24 screws	4020	32160
Expansion chamber front face	16 * 5/16-24 screws	4020	64320

Since the values shown in table 13 are orders of magnitude higher than any pressures which could be reached during the experiment, even in worst case scenarios, the limiting factor would be determined by the low pressure tank, the test chamber, and the acrylic chamber flange. This gives a MAWP = 50 psi, and based on that value the safety factor of the pressure system would be

System Safety factor = MAWP/Max pressure on system = 50/15 psi = 3.3.

Since we have used material yield strength rather than ultimate strength in all of our simulations, this satisfies the minimum safety factor of 2 required in AOD 33897. It should be mentioned that this safety factor for a sudden pressure increase in the system. If the pressure increases slowly, the most likely scenario would be leakage through cracks on the joints of the expansion chamber. We submitted the

consequences of hazardous events in more detail to NASA. We will include those in an appendix. Particular items that refer to vacuum system malfunctions are hazard analysis 1 and 6.

Hazardous Materials

The only working fluid we used in both flights was DCM. A worst case scenario for DCM was calculated, and all quantities and concentrations are well below any dangerous levels.

DCM was chosen due to its relatively high vapor pressure, yet relatively low flammability, surface tension characteristics and several other properties which make it ideal for this experiment. Water was considered as well, and some trial experiments have been conducted with it, but water's low vapor pressure makes it extremely impractical to work with. Another possible candidate was n-pentane, but it is extremely flammable, so it was deemed unsafe. On the other hand, DCM is commonly used as paint thinner, and it is not very flammable.

The amount of fluid needed for an experimental run is about 30 ml (1 fluid ounce). That is the maximum amount of fluid that will be in the aircraft at any given point. Changing fluid types during the flight was discarded since it was extremely impractical. Changing of fluids as well as fluid addition was done on the ground. Since the cabin of the plane is 4700 cubic feet (133 cubic meters), and the air cycles every 3.5 minutes, the fluids, if released at once, would still be below OSHA allowable limits. More detailed information can be found in the table below.

Included below is some MSDS information for DCM which conveys its relative benign characteristics. The complete MSDS for DCM will be included in Appendix B.

Dichloromethane

OSHA Permissible Exposure Limit (PEL): 25 ppm/8hrs TWA; 125 ppm/15mins STEL

Lower Explosive Limit (LEL) 12% in air by volume

Table 14 shows basic properties of the fluids proposed, as well as some of OSHA's permissible limits. As it can be seen, even in the worst case scenario, these fluids, in the quantities that are expected to be aboard the aircraft, will pose no threat to the crew or any researcher.

Table 14. Basic properties and release values of proposed working fluids.

Properties	DCM
Density	1.326 g/cm^3
Molar mass	84.93 g/mol
Freezing/melting point	-96.7 °C
L.E.L	12 %
Mass of fluid in experiment	27.74 g
Moles of fluid in experiment	0.33
Heating value	7.1 MJ/kg
$Vv_{8000'}$	0.37 ft^3 1.1 x 10^{-2} m^3
V_{LEL}	3.1 ft^3 0.09 m^3
D_{Flash}	0.54 m
Energy released at full combustion	197 kJ
PEL LC 50	25 ppm/8hrs 125 ppm/15 min
Release concentration per 3.5 mins	82 ppm

$V_{1\ LEL}$ is the volume that a combusting cloud would have if the amount of fluid of one single experimental run would leak into the cabin and would catch fire. The cabin was assumed to be pressurized at 8000 feet.

D_{Flash} 1 is the diameter that a flashball would have if all the vapor would leak and ignite. Inhalation PEL LC 50 limits are taken from the MSDS of each substance as stated by OSHA. Release concentration shows the amount of fluid present in the cabin if all the liquid would leak at once. As it can be seen, even in the worst case scenario, the concentrations would not reach hazardous limits, and no crew member or researcher would be in danger.

Procedures

The following steps are a simple outline of the operating procedures to follow for the operation of the experiment. We used a more detailed checklist during the actual experimental runs.

Before flight:

1. Mount appropriate bladder according to the fluid to be used.
2. Close the system
3. Inject fluid into the test chamber
4. Condense fluid onto evaporating surface with the dry ice or liquid nitrogen
5. Evacuate until reaching the desired value of non-condensable is reached.
6. Align the schlieren system

During flight:

1. Preheat evaporating surface to specified value and cool condensing surface
2. Decrease system pressure to start evaporation
3. Start data recording process
4. Turn off all vibration-inducing equipment at the beginning of the microgravity cycle
5. Reset during 2 g's cycle.

Emergency Procedures:

1. Turn off power equipment, using switches 1, 2 and 3.
2. Contain and clean-up any spilled fluid.
3. Notify appropriate personnel.
4. Determine if problem can be safely resolved.

5. Reset for continuing experiment if possible, otherwise power down and stow equipment.

Preliminary Results

We successfully flew our experiment, aboard the Zero-G aircraft on two consecutive days. The first flight consisted of mainly troubleshooting while the second flight yielded a large amount of visual, ultrasound, and temperature/pressure data. All mechanical aspects of the system (pump, pressure control, volume-expansion system, heaters/cooler, diagnostics, etc.) functioned as designed. The Martian and Lunar gravity intervals on the second day provided a useful opportunity to establish operating conditions prior to the start of the zero-g parabolae.

The main problem encountered during the flights was the bulk motion of the fluid during the micro-gravity cycles. Figure 12 shows the typical g values experienced during such cycles. It can be easily noticed that though the aircraft remains very close to the intended value of zero g, it is not exactly zero, and those remaining forces impact the fluid behavior. The worst consequence of this is the brief period of time, from about 2 to 4 seconds in the graph, in which the aircraft crosses into a positive value of g. Taking the regular g to be negative, this reach into the positive range is equivalent to briefly turning the test chamber upside down. Since the fluid is not rigidly attached to the aircraft, that resulted in the fluid moving off of the evaporating surface. This was confirmed visually and noted as we were flying. The consequences of such bulk motion meant that we could not thermally control the liquid at the evaporating surface, and most of all, that the proposed experiment of a flat evaporating liquid from a constant temperature surface could not be achieved. We were not actively controlling the chamber walls, hence, when the liquid came into contact with them, it resulted in almost instantaneous boiling.

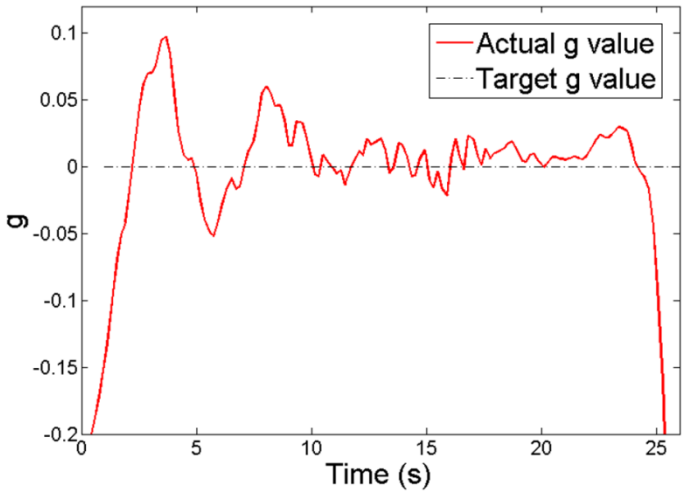

Figure 12. Typical g-loads experienced during a micro-gravity cycle aboard the aircraft

Another undesired side effect of the bulk motion, the boiling, as well as mechanical vibrations from the aircraft itself, tugs and pulls on the rig, and the vacuum pump was a low energy return of the ultrasound signal used to determine the film thickness. Ultrasound techniques have been described before [9] so a thorough discussion will not be included in this dissertation. The typical aircraft post processed file looked as shown in fig 13. In it no film echo is present; hence, no film thickness can be inferred from it.

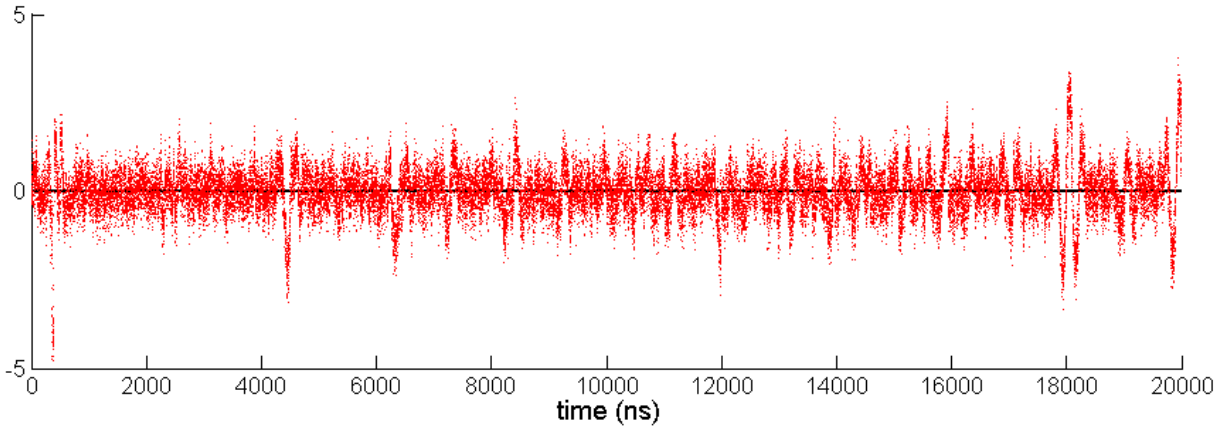

Figure 13. Most representative processed ultrasound reading obtained during flight.

In order to rule out the possibility of a faulty ultrasound system, and to confirm that mechanical vibrations and bulk fluid motions resulted in unusable data file, we ran ground experiments with

undisturbed fluids, and some subject to pump and other mechanical vibrations. When the film was undisturbed, the post processed files yielded great quality fits which can be interpreted, in turn, into the desired film thickness (fig 14).

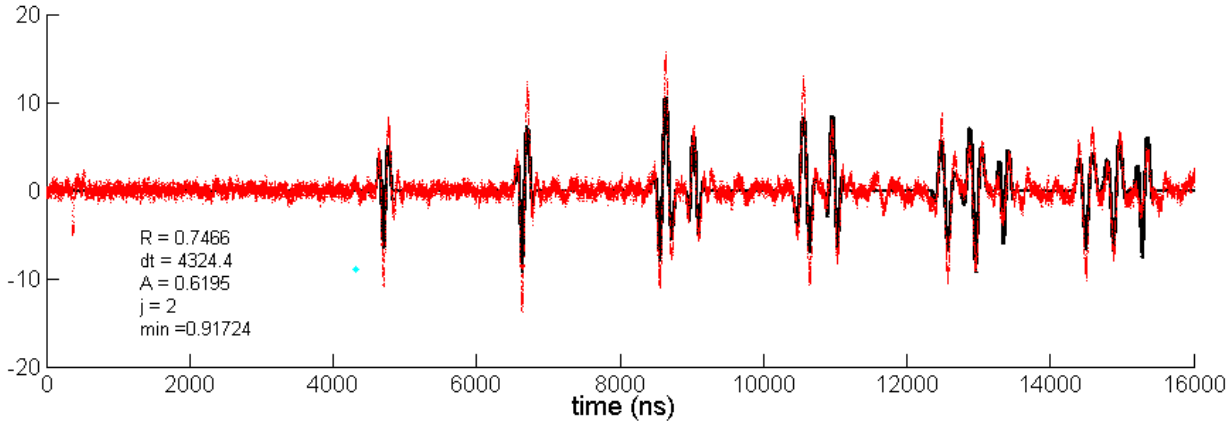

Figure 14. Processed ultrasound signal of a static, undisturbed film in the lab. Thickness is about 4 mm. Acquired signal (red) and simulated signal (black).

Even after turning the pump on, and only shaking the fluid slightly, the signal was still usable (fig 15) though the fitted R value was low.

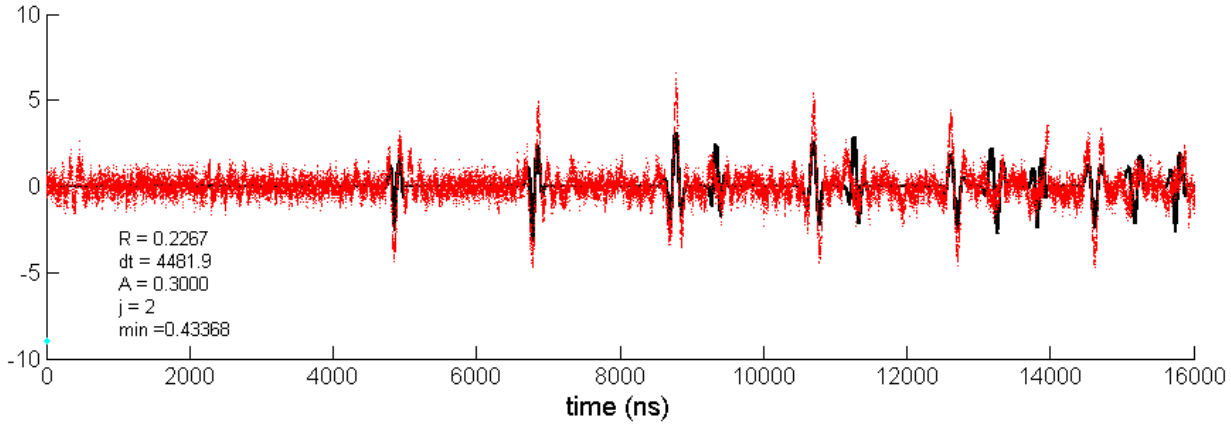

Figure 15. Processed ultrasound signal of a non-evaporating film, with the pump on, and moderately perturbed. Thickness is about 4 mm. Acquired signal (red) and simulated signal (black).

However, once the pump was on, and the system was mechanically perturbed with higher intensity, the data generated was essentially identical to that obtained during flight (fig 16).

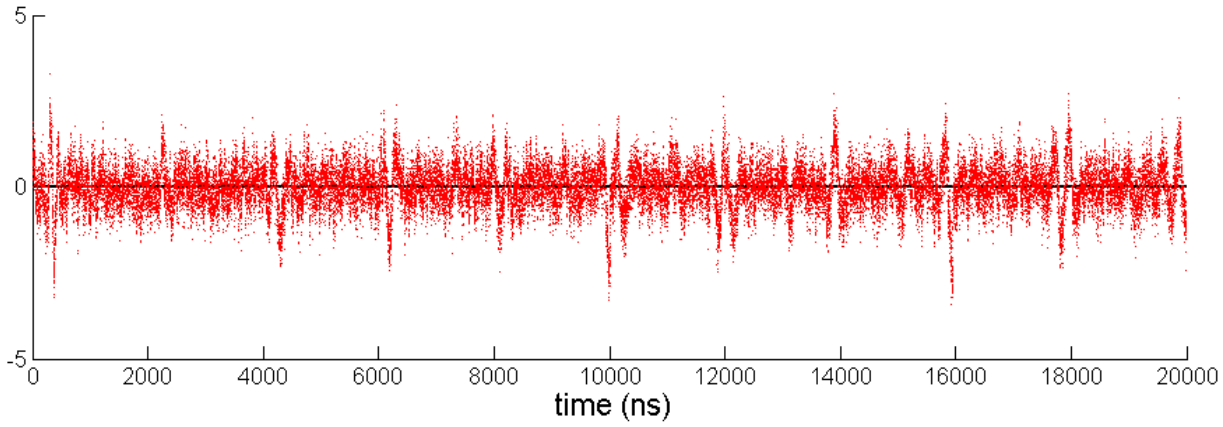

Figure 16. Processed ultrasound signal of a non-evaporating film, with the pump on, and mechanical vibrations. No film thickness can be inferred from the data.

This points at the mechanical vibrations as the main source of errors during flights.

The bulk motion the fluid, which often reached the optical port in zero-g, resulted in unclear and low quality shadowgraph images.

For the reasons mentioned above, which resulted in unstable fluids, the test cell configuration should be redesign in order to ensure the stability of the evaporating films during zero-g intervals. Ultimately, this may point to a long-duration space experiment as the best platform to perform comprehensive studies of film evaporation under microgravity conditions. In that case, films can formed on the desired surface only by condensation, in a fashion similar to that which we have successfully employed in the laboratory at the UW.

By running the experiment in a micro-gravity environment, and carrying out basic tasks during both the reduced-gravity and elevated-g cycles, we now have a much better understanding of the kind of experimental operations that can be done in the aircraft by academic, non-NASA researchers. These experiences will be fully taken into account for the next generation of evaporating-film experiments in reduced gravity. Practical measures should also be considered for the next round of tests in order to improve the loading and unloading of the rig to and from the aircraft, as well as the handling in general. For example, attaching wheels to the rig, and positioning the holes used to attach the system to the aircraft

floor in more accessible places will greatly decrease the effort required to mount the rig aboard the aircraft. We are also planning on some rig re-design to improve accessibility while on board the aircraft, where hardware adjustments can be challenging to make. Certainly, making the rig more accessible will maximize the level of refinement we can achieve and will ensure that we can, with reasonable time and effort, make any necessary adjustments in order to guarantee an optimally-operating system.

Taking into account the numerous ideas for improving the experiment for future reduced-gravity tests will make any second attempts much easier and will greatly improve the conditions needed to obtain great results. The assistance and suggestions from RGO personnel and NASA staff in general as well as from other researchers and Zero-G crew were much appreciated and the entire whole experience was an overwhelmingly positive one.

Future Work

The experiments planned as continuation of the previous work will further explore the heat transfer properties of evaporating films under transient conditions. Our efforts will focus on the following:

- Induce film superheat by heating from below
- Apply successive modulations to the pressure-drop induced superheat. One way this will be achieved is by increasing the superheat in small steps, rather than applying an initial large superheat
- Apply superheat by heating of the wall with similar modulations as the ones previously mentioned.

These proposed experiments will likely produce different results from those obtained by Kimball in which the superheat was applied exclusively by a pressure drop and the wall was kept at a fixed temperature [9]. For example, varying wall temperatures will result in different *Ra* and *Ma* numbers and superheat profiles within the film, which in turn, will likely affect evaporation rate, the surface heat flux and the penetration

depth of the convective structures. The nature of the convective structures is also expected to vary between cases in which the film will be super-heated by heating of the wall from the previously studied experiments in which the super heat has been exclusively applied by a sudden pressure drop.

Works Cited

1. Bénard, H. (1900). “Les tourbillons cellulaires dans une nappe liquide.” Rev. Gen. Sci. Pures Appl, 11, 1261-1271.
2. Rayleigh, L. (1916). “On convection currents in a horizontal layer of fluid when the higher temperature is on the under side.” Philosophical Magazine and Journal of Science, 32, 529-546.
3. Block. (1956). “Surface tension as the cause of Bénard cells and surface deformation in a liquid film.” Nature, 178(4534), 650-651.
4. Pearson, J. R. (1958). On convection cells induced by surface tension. Journal of Fluid Mechanics, 4(5), 489-500.
5. Nield, D. A. (1964). Surface tension and buoyance effects in cellular convection . Journal of Fluid Mechanics, 19(July), 341-352.
6. Sternling, L. E. (1964). On cellular convection driven by surface-tension gradients: effects of mean surface tension and surface viscosity. Journal of Fluid Mechanics, 19(03), 329-340.
7. Busse, F. H. (1978). “Non-linear properties of thermal convection.” Reports on Progress in Physics, 41(12), 1929-1965.
8. Velarde, M. G. (1982). Buoyancy-thermocapillary instability - the role of interfacial deformation in one-component and 2-component fluid layers heated from below or above. Journal of Fluid Mechanics, 125(Dec), 463-474.
9. Kimball, J. (2010). “Interfacial stability, convective structure and heat transfer in liquid films undergoing phase change.” University of Washington, 2010.
10. Touazi, O. C. (2010). Simulation of transient Rayleigh-Bénard-Marangoni convection induced by evaporation. Journal of Heat and Mass Transfer, 53, 656-664.
11. Koschmieder, E. L. (1993). Bénard Cells and Taylor Vortices. Cambridge University Press.
12. Chandrasekhar, S. (1961). Hydrodynamic and Hydromagnetic Stability. Clarendon Press.

Appendix A. Structural Verification

Introduction

This document covers the rest of the structural analysis which was not addressed in the TEDP. The procedure for the analysis themselves will be done just as outlined in the TEDP. Basically we will establish the maximum allowable load for a given bracket, add all the brackets in the given system being analyzed, and compare it with the maximum expected load.

The maximum allowable working loads were obtained by either the manufacturer directly, pull tests, or numerical analysis, typically done in ANSYS. Even some of the manufacturer values were checked experimentally and were found at times to differ greatly from observations. It should also be pointed out that bracket were found to fail at lower loads than screws or the frame itself. We will not in the cases were the failure of a system is determined by buckling of beams, or shearing or stripping of bolts, although these account for a small minority of situations.

Pull Tests

As mentioned in the main text of the data package, the first step was to determine the failure elements and limits for the experimental frame and joints. In most cases the failure element consisted of the bracket used in the joint either sliding or deforming. Other limits such as stripping or shearing of the screws were considered. It should also be noted that the limits shown are not necessarily breaking limits. They are limits which we either physically tested, or ran simulations, hence we know are safe limits at which failure would not occur.

Two kinds of pull tests were done, one done mostly do determine the maximum turning moment brackets could withstand, and another one to determine force required to slide a bracket system. Test documentation for each of the test is given below.

Pull Test 1

In compliance with AOD 33896, section 2.11.2, required experimental pull test documentation as applied to the first kind of pull tests, is shown below.

A. The pull tests were performed by attaching the test specimen to an 80-20 fixed beam, while the other end was attached to a cantilevered section. The latter one was then pulled with a force gauge, or weights were hung from it. The distance at which the load was applied was recorded A picture of the test set up is shown in figure 1. The pull (or weights) were increased in incremental steps while recording the deflection (or sliding) of the bracket. Once plastic deformation was registered, the value of the load was recorded, resulting on a moment tolerance for the part. Most pull tests performed were aimed at obtaining a tolerance for moment loads because the loads required were relatively small. Pull tests for direct force were avoided because they would have required much larger loads.
B. A commercial force gauge was used, for most pull tests. The gauge was calibrated with known weight standards, and zeroed before each test. A minority of the tests were done by hanging the weights directly on the beam. Deflections were measured with a commercial metric tape.

C. Tests were performed Juan Carlos Gonzalez, one of the PI's of the project.

D. N/A

E. Does not apply. Tests were done in order to obtain a maximum limit for the part being tested. That value was then used to calculate the maximum tolerance in the applicable load configuration.

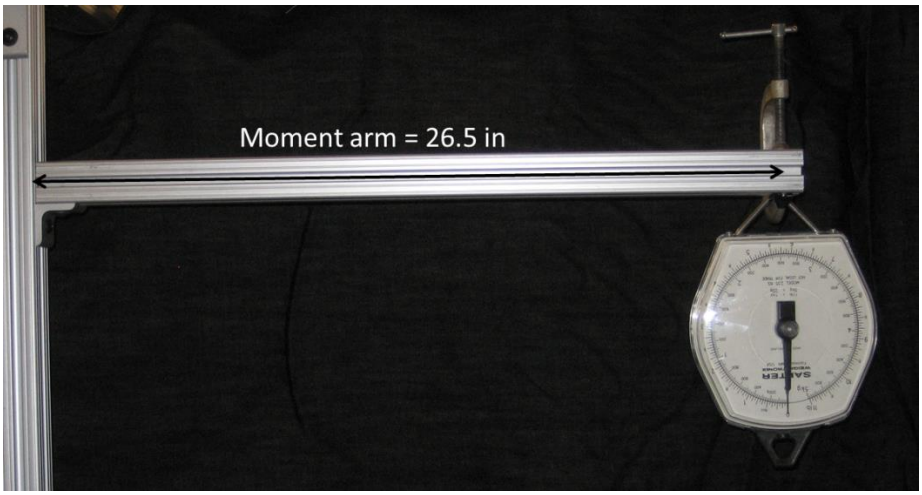

Figure A1.17. Pull test set up for the 4302 bracket. Similar set ups were made for all other instances.

Pull Test 2

In compliance with AOD 33896, section 2.11.2, required experimental pull test documentation which applies to the pull tests done to establish the force required to slide a 2 bracket system.

A. This pull tests was performed by fixing one end of the two bracket system to an Instron 8801 machine while the other end held the piece to be analyzed. Even though we call it a "pull" test, in reality we pushed the piece in order to obtain the force it takes to slide the particular piece. The test was performed on three types of brackets: 4301, 4302 and a slotted 2-bracekt system. The results of the 4301 and 4302 apply to anything attached to the 8020 beams with two and one bolt respectively. Figure 2 shows a picture of this pull test set up.

B. The test equipment employed was an Instron 8801 and 8800 gauge. The calibration was done with an internal shunt system, following manufacturer specifications.

C. Tests were performed Robert Gordon and Juan Carlos Gonzalez.

D. N/A

E. Does not apply. Tests were done in order to obtain a maximum limit for the part being tested. That value was then used to calculate the maximum tolerance in the applicable load configuration.

Figure A1.18. Test of sliding force resistance on a 4301 bracket.

Brackets and Joints Tolerances

This section show the breaking limits (or the maximum tested load) of the parts used in the assembly, accompanied by a sketch clarifying the mode. A legend will be introduced as well so that it can be easily referenced in the calculations. It should be pointed out that some values were obtained from 80-20. Most of those values were checked in the lab and/or with finite element solvers. The values included in this report are those values closest to the experimental results.

3330

The 3330 bolt sold by 80-20 was the bolt of choice used to assemble the frame and to fix parts to the structure. The bolt is a 5/16-18, made of alloy steel with black zinc finish. In most cases, when bolts are used with 80-20 brackets, or even custom made brackets, the failure limit of the bolt-bracket system will be determined by the bracket, unless otherwise indicated. In a few cases, for example, in attaching the bottom Aluminum plate to frame, the 3330 bolts will be used to attach the part directly to the 80-20 beams, so the failure limit, either in sliding, shearing or striping, will be determined by the bolts. Since 80-20 does not provide failure limits for this part, the limits were obtained by pull tests and the MIL-HDBK5 manual. The bolt can be used in conjunction with a wide array of T-nuts, also sold by 80-20. Below is shown the 3330 bolt with the most common t-nut used in the assembly. It should be noted as well that in order to get consistent and repeatable failure values, particularly in the sliding configuration, since it is based in friction, the bolt will be tightened with a torque wrench to the specified value of 15 ft-lbs.

Part and mode: 3330 sliding

Nomenclature: 3330 sl

Failure point: 600 lbs (Pull Test)

Failure cause: Sliding of the part

Part and mode: 3330 shearing

Nomenclature: 3330 sh

Failure point: 2730 lbs (MIL-HDBK5)

Failure cause: Shearing of the bolt

Part and mode: 3330 striping

Nomenclature: 3330 st

Failure point: (MIL-HDBK5)

Failure cause: Striping of the bolt

3095

The 3095 joint, or double anchor, can withstand some of the highest loads among the available joining methods offered b 80-20. The implementation of this anchor provided the extra support needed to satisfy the 9 g's forward loading requirement, especially when dealing induced turning moments.

Part and mode: 3095 Shear Force 1

Nomenclature: 3095s1

Failure point: 1200 lbs (Manufacturer)

Failure cause: Unspecified

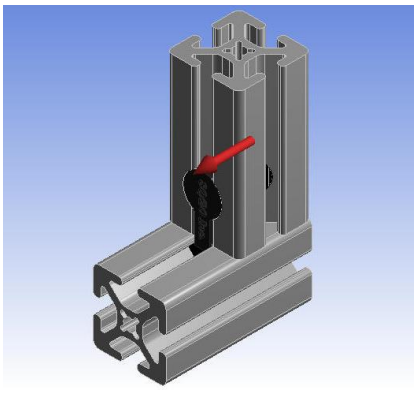

Part and mode: 3095 Shear Force 2

Nomenclature: 3095s2

Failure point: 1200 lbs (Manufacturer)

Failure cause: Unspecified

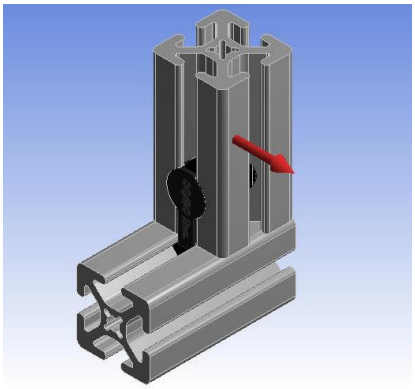

Part and mode: 3095 Shear Force 3

Nomenclature: 3095s3

Failure point: 8040 lbs (MIL-HDBK5)

Failure cause: Tensile breaking point of the screws in the anchor (Deformation of the beams occurs at higher loads when checked in ANSYS)

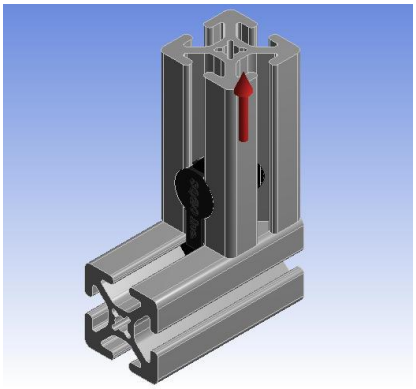

Part and mode: 3095 Moment 1

Nomenclature: 3095m1

Failure point: 7200 in- lbs (Manufacturer)

Failure cause: Unspecified

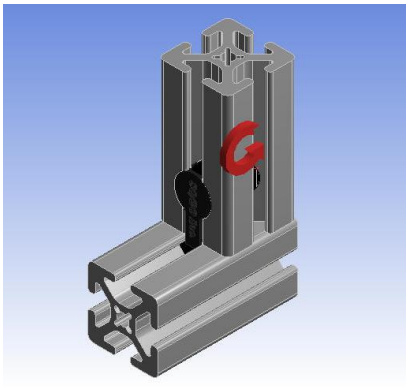

Part and mode: 3095 Moment 2

Nomenclature: 3095m2

Failure point: 7200 in- lbs (Manufacturer)

Failure cause: Unspecified

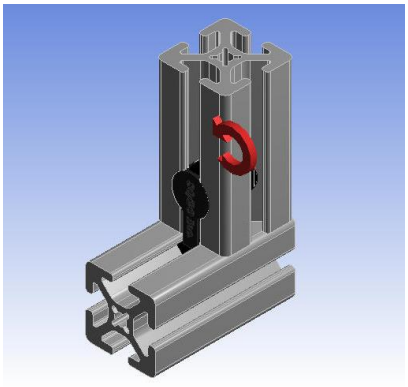

Part and mode: 3095 Moment 3

Nomenclature: 3095m3

Failure point: 2000 in- lbs (Manufacturer)

Failure cause: Unspecified

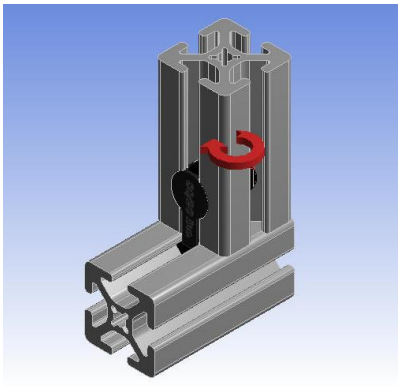

4301

The 4301 bracket was used extensively in the rig, particularly in locations where high turning moments were not expected. This section shows the maximum loads it can tolerate for different loading configurations.

Part and mode: 4301 Shear Force 1

Nomenclature: 4301s1

Failure point: 1200 lbs (Pull Test)

Failure cause: Sliding of the T-nut-screw-bracket system

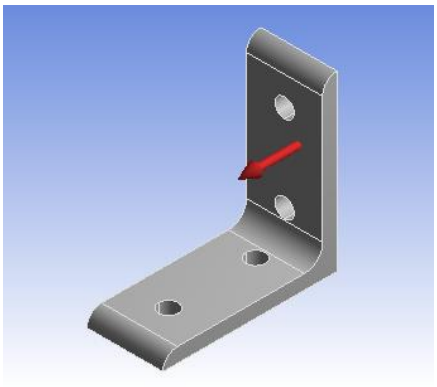

Part and mode: 4301 Shear Force 2

Nomenclature: 4301s2

Failure point: 5400 lbs (MIL-HDB5)

Failure cause: Bearing strength of the bracket.

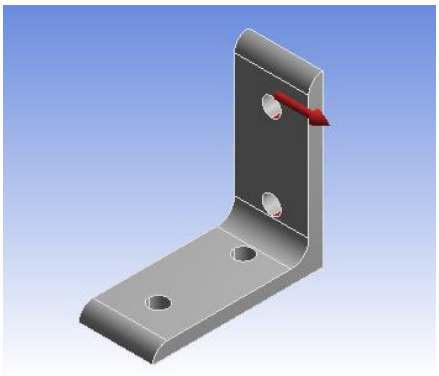

Part and mode: 4301 Moment 1

Nomenclature: 4301m1

Failure point: 500 in- lbs (Pull test corroborated by ANSYS)

Failure cause: Plastic deformation of the bracket

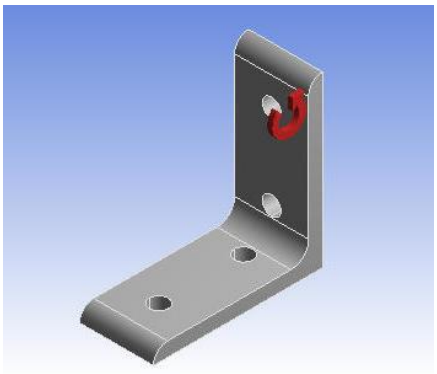

Part and mode: 4301 Moment 2

Nomenclature: 4301m2

Failure point: 500 in- lbs (Pull test corroborated by ANSYS)

Failure cause: Plastic deformation of the bracket

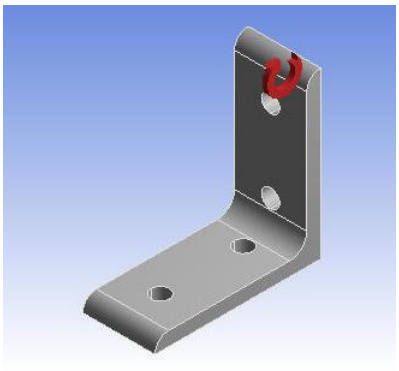

Part and mode: 4301 Moment 3

Nomenclature: 4301m3

Failure point: 1000 in- lbs (Pull test corroborated by ANSYS)

Failure cause: Tearing of the bracket at the “hinge”

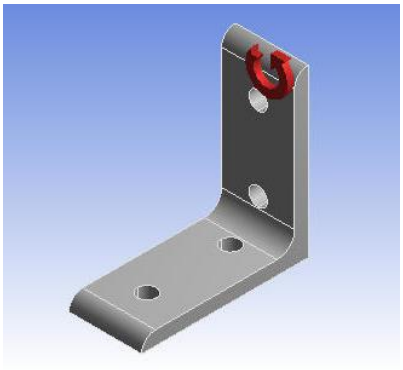

4302

The 4302 bracket was used primarily when attaching beams to systems with expected lower loads. Due to the fact that this bracket only has one bearing in each beam, makes it prone to sliding out. Notice the big difference in the loads it can withstand between the Shear Force 1 and the Shear Force 2.

Part and mode: 4302 Shear Force 1

Nomenclature: 4302s1

Failure point: 600 lbs (Pull Test)

Failure cause: Sliding of the T-nut-screw-bracket system

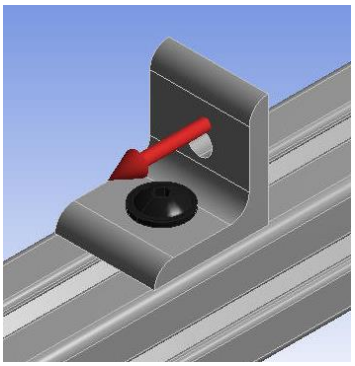

or

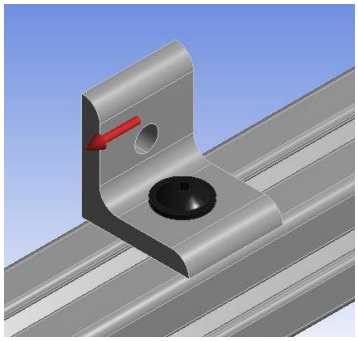

Part and mode: 4302 Shear Force 2

Nomenclature: 4302s2

Failure point: 2730 lbs (MIL-HDBK5)

Failure cause: Breaking of the screw hole

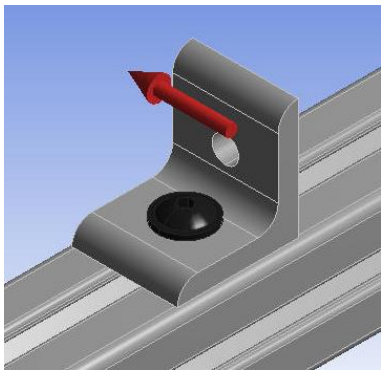

or

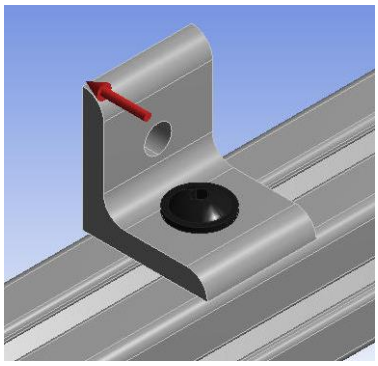

Part and mode: 4302 Moment 1

Nomenclature: 4302m1

Failure point: 420 in- lbs (Pull test corroborated by ANSYS)

Failure cause: Plastic deformation of the bracket

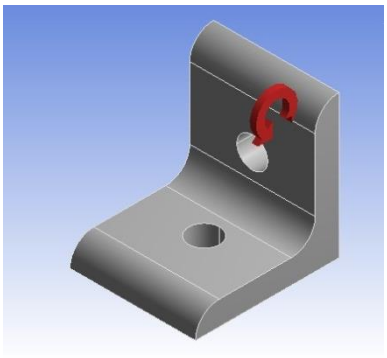

Part and mode: 4302 Moment 2

Nomenclature: 4302m2

Failure point: 400 in- lbs (ANSYS)

Failure cause: Plastic deformation of the bracket

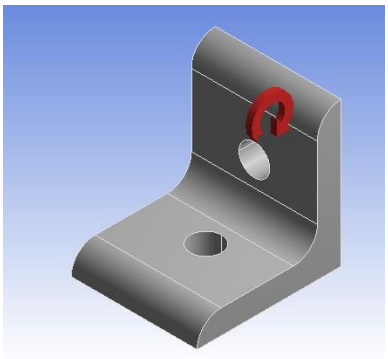

Part and mode: 4302 Moment 3

Nomenclature: 4302m3

Failure point: 240 in- lbs (Pull test)

For Failure cause: Sliding of the beam out of the T-nut and screw

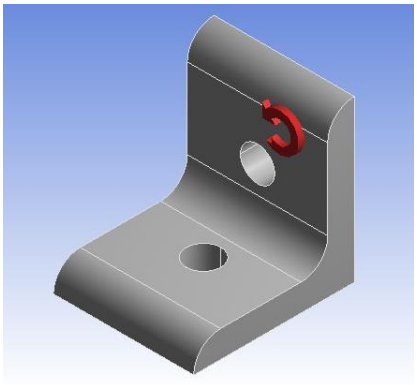

Or

Failure point: 800 in- lbs (ANSYS)

For Failure cause: Tearing of the bracket holes

(This second version occurs when one end hole of the bracket attached to a 1515 beam, and the other hole is attached to a

different part which can restrain the screw-T-nut system. In this case the value is higher because the screw-nut system cannot slide; hence we get the “true” limit of the bracket rather than the sliding of the nut. This case will be referenced as 4302m3h)

Part and mode: 4302 Moment 4

Nomenclature: 4302m4

Failure point: 160 in- lbs (Pull test)

Failure cause: Rotation of the bracket

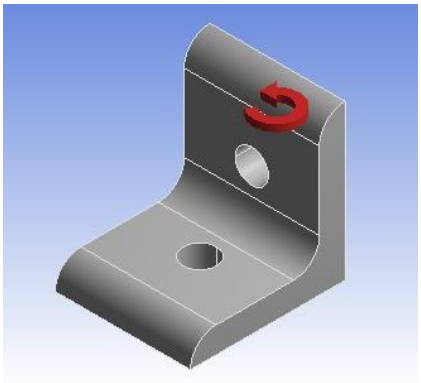

4376

The 4376 bracket is essentially a hybrid between the 4301 and 4302. Hence, we will reference values conservatively to the 4302, except in those cases where it will obviously behave like the 4301 bracket.

Part number: 4376

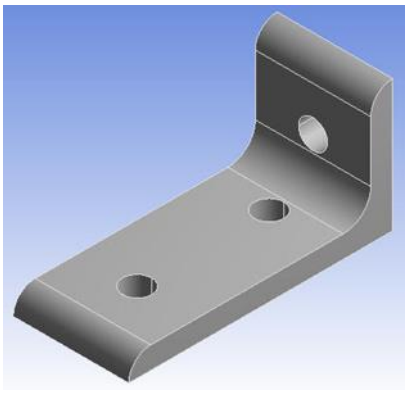

4336

This bracket offers the structural stability of "triangles" in the frame. It can withstand fairly high loads, yet it is still compact and allows for a high level of accessibility to experimental equipment.

Part and mode: 4336 Shear Force 1

Nomenclature: 4336s1

Failure point: 1200 lbs (Pull Test)

Failure cause: Sliding of the T-nut-screw-bracket system

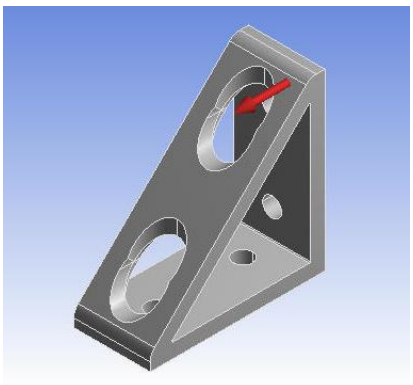

Part and mode: 4336 Shear Force 2

Nomenclature: 4336s2

Failure point: 5400 lbs (MIL-HDBK5)

Failure cause: Breaking of fixed bracket holes

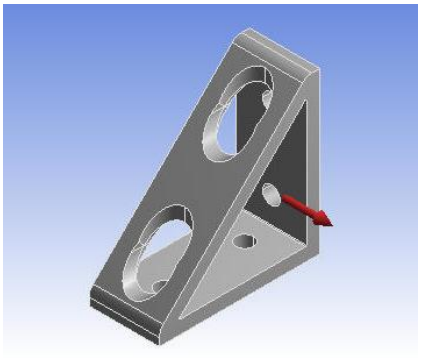

Part and mode: 4336 Moment 1

Nomenclature: 4336m1

Failure point: 4000 in-lbs (Manufacturer and checked by ANSYS)

Failure cause: Plastic deformation of the bracket

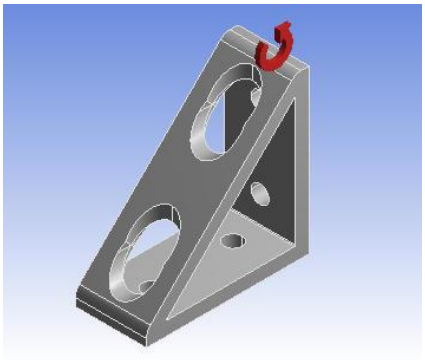

Part and mode: 4336 Moment 2

Nomenclature: 4336m2

Failure point: 3700 in-lbs (ANSYS)

Failure cause: Tearing of the gusset at the thinnest point

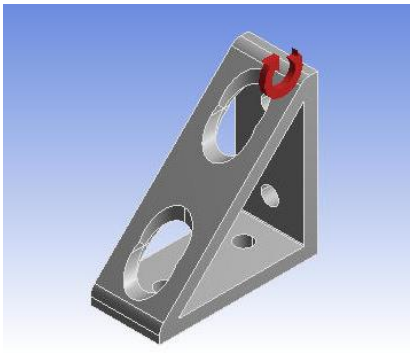

Part and mode: 4336 Moment 3

Nomenclature: 4336m3

Failure point: 1200 in-lbs (ANSYS)

Failure cause: Tearing of the bracket at the hinge

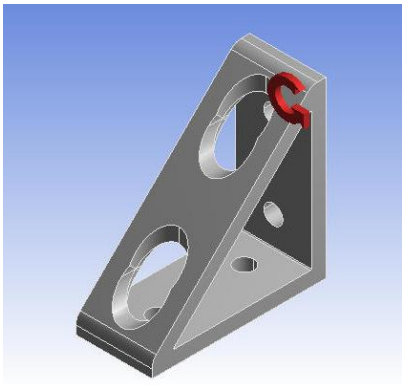

4332

The modified version of the 4332 was introduced in order to match the load requirements of the chamber system. The modification consists of extending the hole on one of the sides so that it can be mounted on the long rods holding the expansion chamber. It is essentially the only place where they are used. Since the load it takes to make them slide depends on the beams and screw-T-nut system, the shear force tolerances are identical to the 4302 bracket. Hence, only the turning moment tolerances will be included in this section.

Part and mode: 4332M Moment 1

Nomenclature: 4332Mm1

Failure point: 3000 in- lbs (ANSYS)

Failure cause: Plastic deformation of the bracket at the gusset

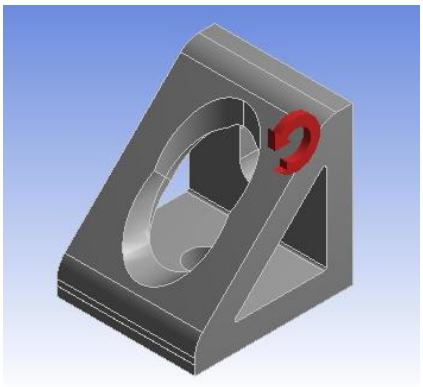

Part and mode: 4332M Moment 2

Nomenclature: 4332Mm2

Failure point: 2500 in- lbs (ANSYS)

Failure cause: Tearing of the bracket at the gusset

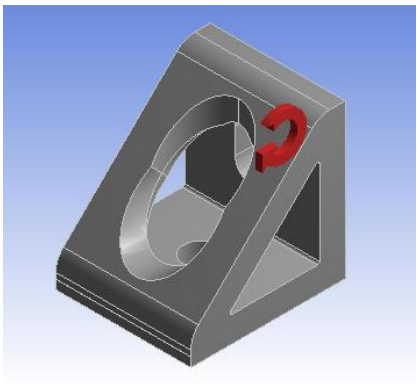

Part and mode: 4332M Moment 3

Nomenclature: 4332Mm3

Failure point: 1000 in- lbs (ANSYS)

For Failure cause: Plastic deformation of the bracket at multiple points

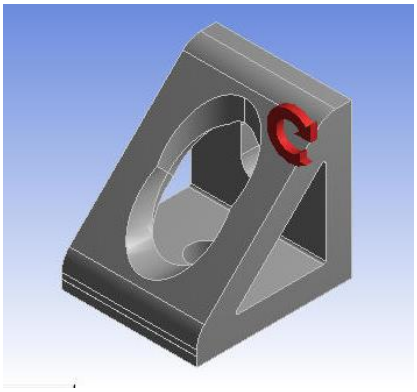

2 Slot Expansion Chamber Bracket

Part and mode: 2 slot chamber bracket

Nomenclature: 2SBs1

Failure point: 1200 lbs (Pull Test)

Failure cause: Sliding of the bracket

(* Although that is not an 80-20 part, we are using the same values since 500 lbs is the amount of force it takes to slide two bolts on the frame)

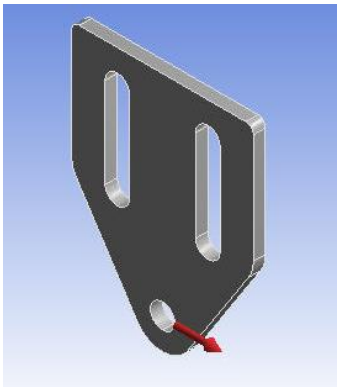

Part and mode: 2 slot chamber bracket

Nomenclature: 2SB m1

Failure point: 600 in-lbs (Pull test)

Failure cause: Plastic deformation of bracket

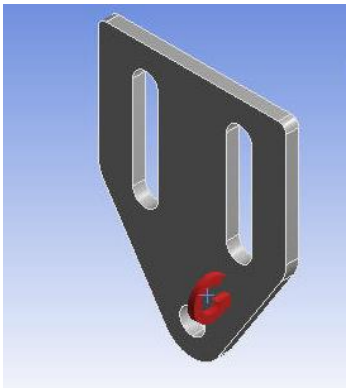

Slotted Bracket System

Part and mode: Slotted bracket system Shear Force 1

Nomenclature: SBSs1

Failure point: 575 lbs (Manufacturer*)

Failure cause: Sliding of the T-nut-screw-bracket system

(* Although that is not an 80-20 part, we are using the same values since 500 lbs is the amount of force it takes to slide two bolts on the frame)

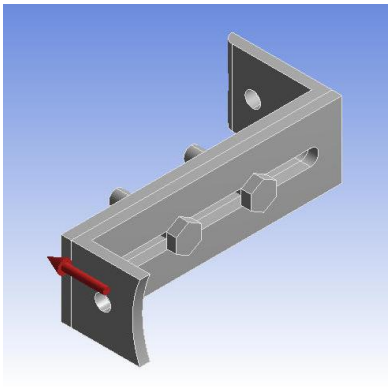

Part and mode: Slotted bracket system Shear Force 2

Nomenclature SBSs 2

Failure point: 800 lbs (ANSYS)

Failure cause: Tearing of the bracket slots.

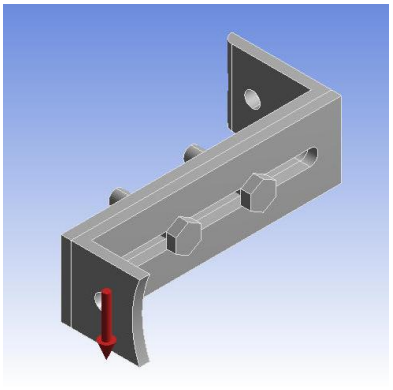

Part and mode: Slotted bracket system Shear Force 3

Nomenclature SBSs 3

Failure point: 300 lbs

Failure cause: Sliding of the brackets

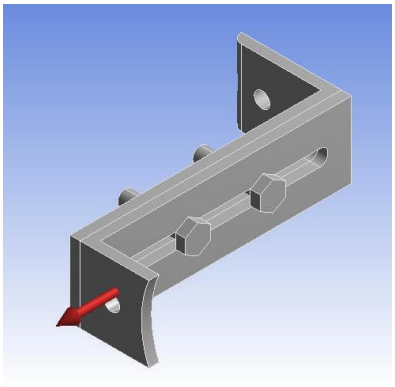

Part and mode: Slotted bracket system Moment 1

Nomenclature: SBSm1

Failure point: 200 in-lbs (Pull tets)

Failure cause: Plastic deformation of the bracket

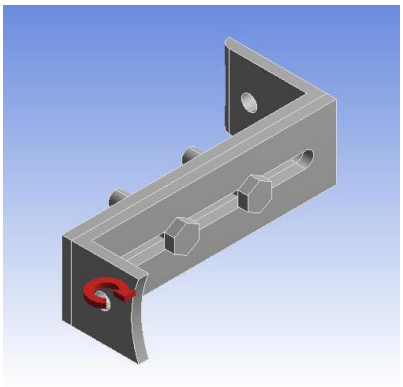

Part and mode: Slotted bracket system Moment 2

Nomenclature: SBSm2

Failure point: 250 in-lbs (Pull test)

Failure cause: Plastic deformation of the bracket

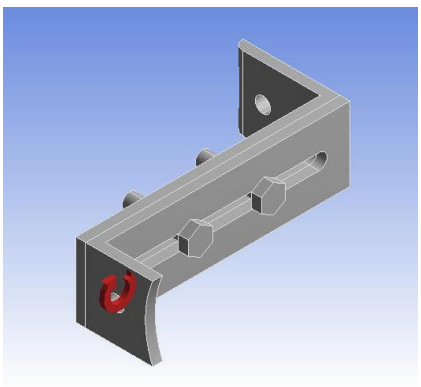

Reinforcing Pump Bracket

This bracket was introduced in order to help withstand the relatively high load induced by the vacuum pump. Since this high load is mostly due to the turning moment of the pump under the 9 g's

forward condition, the bracket only needs one bearing, through which it will be attached to the frame. The other end of the bracket will be pressing down on the base of the pump. This will be shown in more detail in a section dedicated specifically to the pump.

Part and mode: Reinforced pump bracket force

Nomenclature: EPBs1

Failure point: 800 lbs (ANSYS)

Failure cause: Plastic deformation of bracket

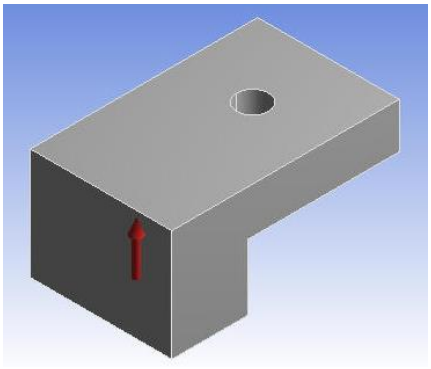

Part and mode: Reinforced pump bracket moment

Nomenclature: EPBm1

Failure point: 3100 in-lbs (ANSYS)

Failure cause: Plastic deformation of bracket

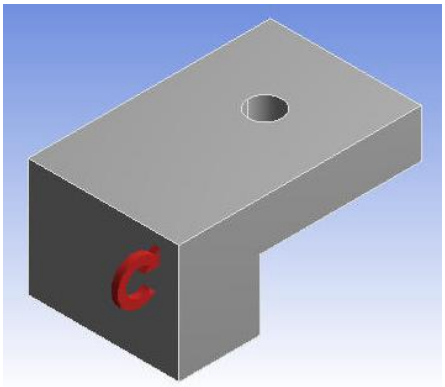

Frame and Assemblies Analysis

One assumption which facilitated the process of the structural analysis was that of equal loading at each joint. In reality, the structure is statically indeterminate, but beams are highly interconnected, so the load is shared fairly evenly by all members. For example, the scope is attached directly to the top longitudinal beam and a top transverse beam. The top longitudinal member transfers the loads evenly through the vertical beams, and the transverse beam, which is attached to the front longitudinal member, also transfers the load to the bottom through the vertical beams.

The following shows the rest of the calculations done to comply with the structural analysis requirement. The frame figures will be presented again, in order to provide quick access to the references and nomenclature. The format of the analysis will be the same for all parts analyzed. A table showing the calculation of the limit of the frame, or part, being analyzed will be shown first, followed by a second table in which the safety factor will be calculated based on the limit, and the expected loading.

The general orientation of frames analyzed in the following sections will abide by the configurations shown in figure 3. The forward axis subject to the 9 g loading condition will always be pointing obliquely into the page, and the aft direction, subject to the 3 g loading condition, will be opposite, out of the page.

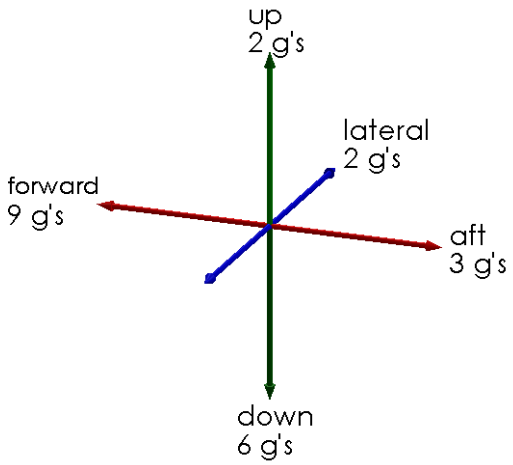

Figure A1.19. Axis orientation as it applies to frames shown in present document.

Bottom Section

The vertical beam junctions along the bottom of the frame carry the highest load induced by the equipment. These junctions were redesigned with 4336 gussets and 3095 double anchors in order to meet the safety factor of 2, specifically for the 9 g's forward loading requirement. The 9 g's requirement was already addressed in the TEDP. What follows here is the analysis of the remaining loading conditions. Figure 4 shows the labeling system to be used when referencing the joints of the vertical beams at bottom frame. The consequent tables show the tolerances of such junctions to a particular load, and the resulting safety factors.

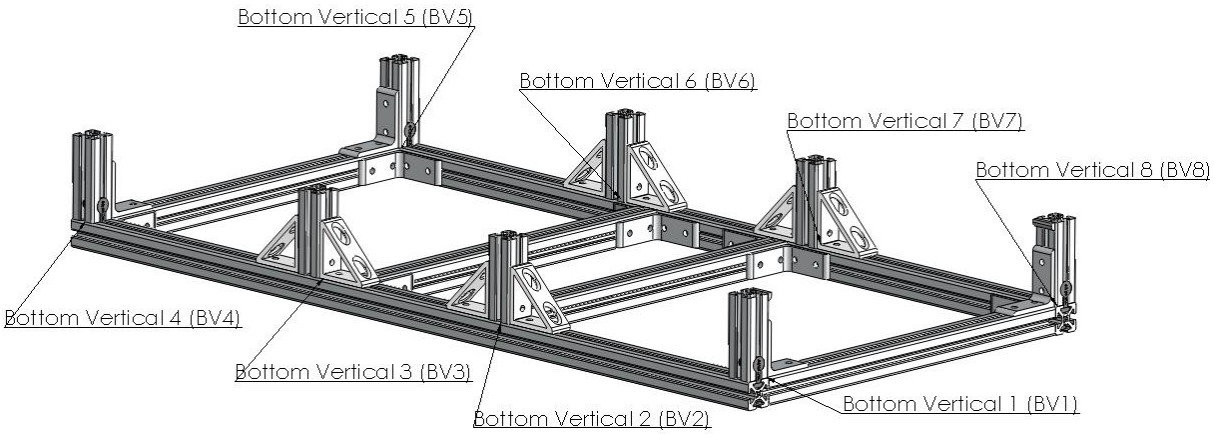

Figure A1.20. Vertical beam junctions along the bottom of the frame

Table A1.15. Vertical beam junctions along the bottom tolerances and safety factor for the 6 g's downward load condition

Bottom tolerances for downward loads				
Junction		Joining method	Failure mode	Failure force (lbs)
BV1		fixed end	beam buckling	30000
BV2 - BV8		Same	beam buckling	210000
Total				**240000**

6 g's downward loading condition		
Frame limit (lbs)		240000
loading under 6 g's downward (lbs)		1741
Safety Factor		138

Table A1.16. Vertical beam junctions along the bottom tolerances and safety factors for the 2 g's lateral load condition

Vertical beams bottom junctions tolerance along the lateral line						
Junction		Joining Method	Shear failure mode	Max allowable shear force (lbs)	Moment failure mode	Max alloawable moment (in-lbs)
BV1		3095	3095s2	1200	3095m1	7200
		1 * 4301	4336s1	1200	4336m1	4000
BV2		2 * 4336	4336s2	10800	4336m3	2400
BV3		Same as BV2	(see above)	10800	(see above)	2400
BV4		Same as BV1	(see above)	2400	(see above)	11200
BV5		Same as BV1	(see above)	2400	(see above)	11200
BV6		Same as BV2	(see above)	10800	(see above)	2400
BV7		Same as BV2	(see above)	10800	(see above)	2400
BV8		Same as BV1	(see above)	2400	(see above)	11200
Total				**52800**		**54400**

2 g's lateral loading condition						
Force limit (lbs)		52800		Moment limit (in-lbs)		54400
Force under 2 g's lateral loading (lbs)		496		Moment under 2 g's lateral loading (in-lbs)		7993
Safety factor (Force)		107		Safety factor (Moment)		7

Table A1.17. Vertical beam junctions along the bottom tolerances and safety factors for the 2 g's upward load condition

Vertical beams bottom junctions tolerance for upward loading conditions				
Junction		Joining method	failure mode	failure force (lbs)
BV1		3095s3	stripping of screw	8000
		4301	4301s1	1200
BV2		2 * 4336	4336s1	2400
BV3		Same as BV2	4336s1	2400
BV4		Same as BV1		9200
BV5		Same as BV1		9200
BV6		Same as BV2	4336s1	2400
BV7		Same as BV2	4336s1	2400
BV8		Same as BV1		9200
Total				**46400**

2 g's upward loading condition		
Bottom junctions limit (lbs)		46400
2 g's upward loading (lbs)		580
Safety Factor		80

Sides and top

The safety factors of this portion of the frame under the 9 g's forward load were calculated on the main text of the TEDP. What follows here is the calculation of the safty factors for the rest of the loading configurations. Figure 5 shows the lableing nomenclature which will be followed. Tables 4 and 5 show the junctions (or beams) tolerances in a given direction and the calculated safety factors.

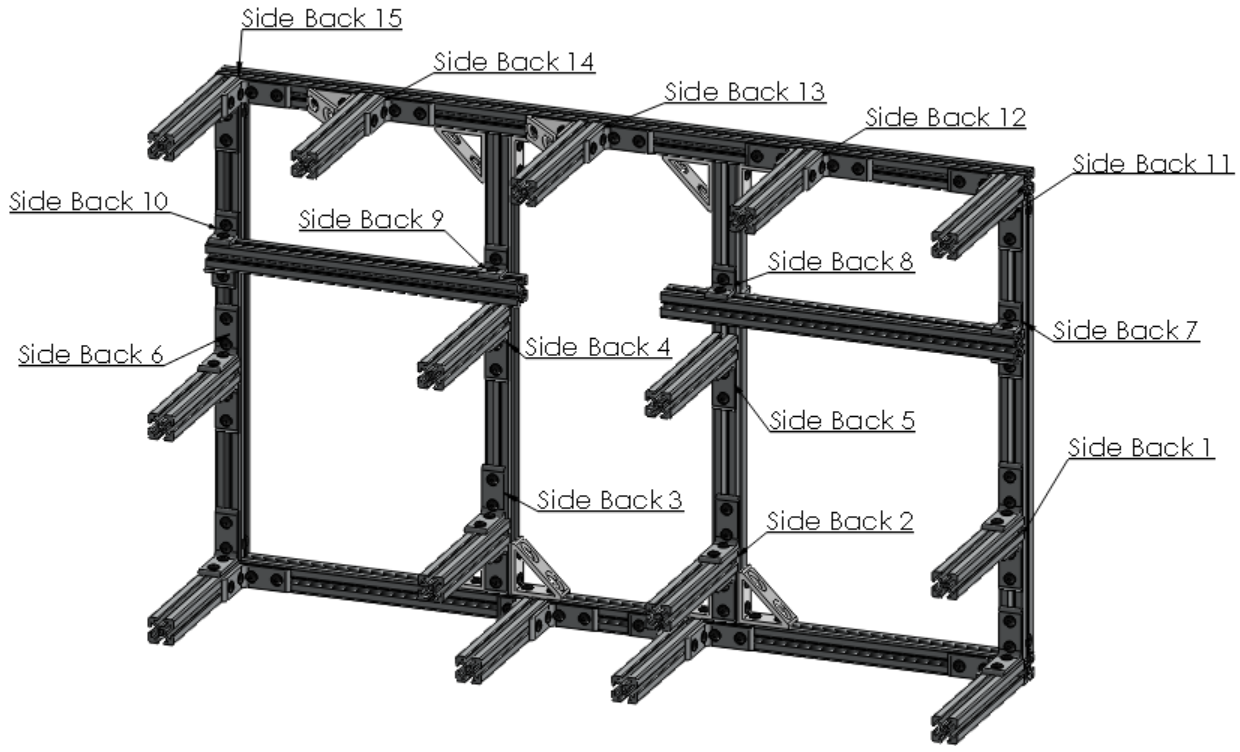

Figure A1.21. Sketch and nomenclature of the sides and top section of the frame

Table A1.18. Sides and top tolerances and safety factor for the 6 g's downward load condition

Top and sides tolerances for donward or upward loading						
Junction		Brackets	Shear failure mode	Max allowable shear force (lbs)	Moment failure mode	Max alloawable moment (in-lbs)
Side Back 1		2 * 4301	4301s1	1200	4301m1	1000
Side Back 2		Same as SB1	4301s1	1200	4301m1	1000
Side Back 3		Same as SB1	4301s1	1200	4301m1	1000
Side Back 4		1 * 4301	4301s1	600	4301m1	1000
Side Back 5		Same as SB 4	4301s1	600	4301m1	1000
Side Back 6		Same as SB1	4301s1	1200	4301m1	1000
Side Back 7		2 * 4302	4302s1	1200	n/a	
Side Back 8		1 * 4302	4302s1	600	n/a	
		2 * 4302	4302s1	1200	n/a	
Side Back 9		1 * 4302	4302s1	600	n/a	
		1 * 4302	4302s1	600	n/a	
Side Back 10		2 * 4302	4302s1	1200	n/a	
Side Back 11		1 * 4301	4301s2	5400	4301m3	1000
		1 * 4301	4301s1	1200	4301m1	500
Side Back 12		2 * 4301	4301s2	10800	4301m3	2000
Side Back 13		1 * 4301	4301s2	5400	4301m3	1000
		1 * 4336	4336s2	5400	4336m3	1000
Side Back 14		Same as SB 13	(see above)	10800	(see above)	2000
Side Back 15		Same as SB 11	(see above)	6600	(see above)	1500
Total for SB				57000		15000
		Side Front equal to Side Back				
Total				**114000**		**30000**

6 g's downward loading condition						
Limit in force (lbs)		114000		Top and sides moment limit (in-lbs)		30000
Force under 6 g's forward loading (lbs)		798		Moment under 6 g's forward loading (in-lbs)		9177
Safety factor (Force)		143		Safety factor (Moment)		3

The previous configuration automatically satisfies the 2 g's upward loading condition.

Table A1.19. Sides and top tolerances and safety factors for the 2 g's lateral load condition

Top and sides tolerances for lateral loads				
Junction		Joining method	failure mode	failure force (lbs)
Side Back 1		fixed end	beam buckling	30000
SB2 - SB 15		Same	beam buckling	420000
Total				**450000**

2 g's lateral loading condition		
Beam limits (lbs)		450000
2 g's lateral load (lbs)		266
Safety factors		1692

Bottom Plate

An Aluminum plate 0.25 in thick will serve as the base of the frame. Having an Aluminum base will add rigidity, and it will make attaching the experiment to the floor of the aircraft easier to carry out. As discussed in the main text of the TEDP (item 5) we have to calculate the load that the rest of the system will exert on the plate to make sure that the frame will not slide out of the Aluminum base. This part of the analysis was done in the same fashion as the other calculations in this report.

We also have to make sure that the Aluminum base can withstand the load of the entire experiment, including itself. The footprint of our system, and size of the Aluminum base is 24 by 48 inches. Given that the bolt pattern on the floor of the aircraft is 20 by 20 inches, the maximum number of attachment points we can have is 6. This part of the analysis was done numerically, given that we only have the Aluminum plate to study, rather than a complex array of different brackets such as in most cases

in this report. The loading on the bolts provided by Zero-G to attach the experiment to the floor and the load on the floor itself will be verified in the next section.

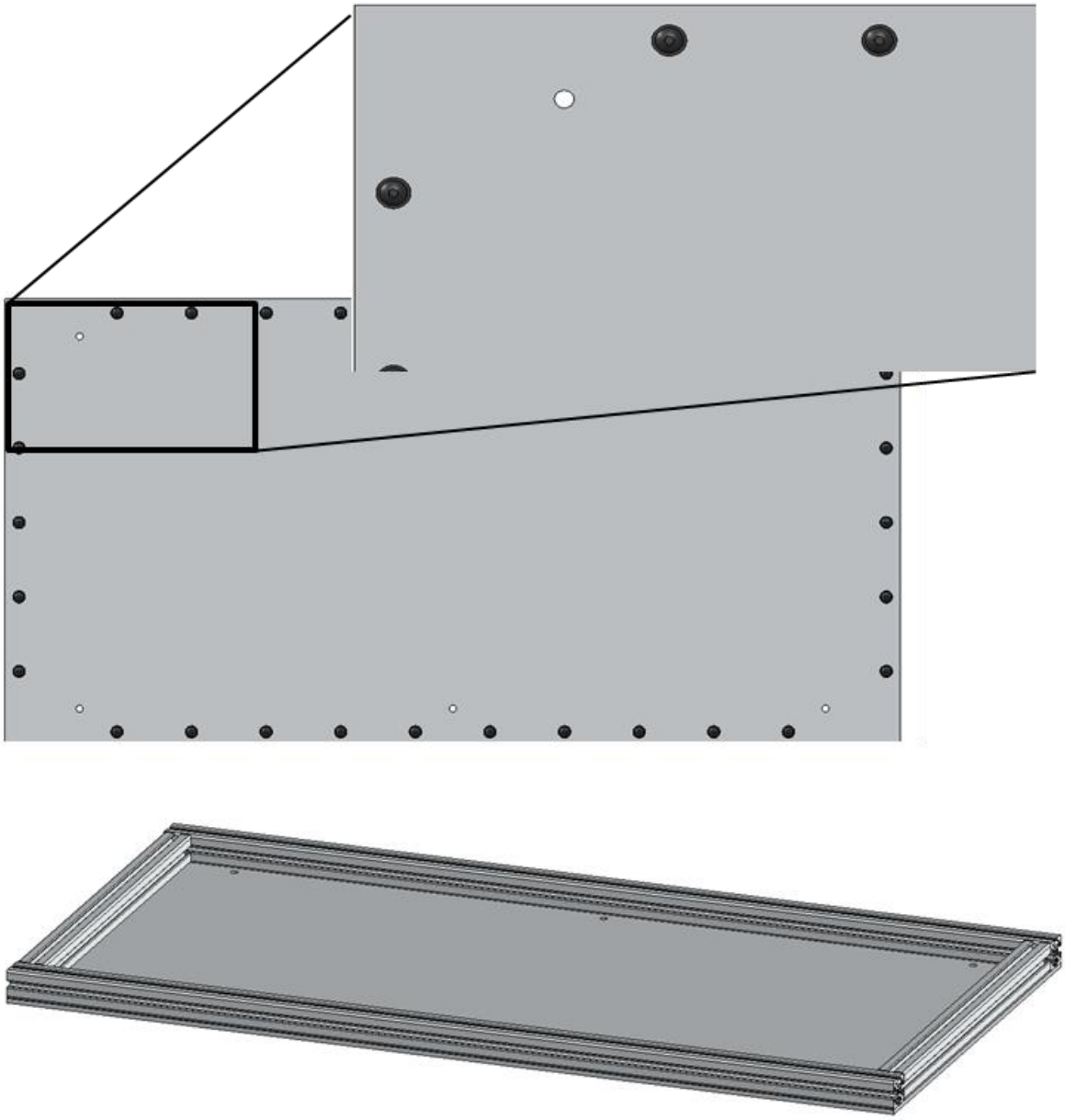

Figure A1.22. Aluminum base viewed from the bottom with zoom on the corner to highlight the bolts (top) and diametric view with the bottom beams visible (bottom)

Table A1.20. Tolerances and safety factor calculations for the loads of the frame on the Aluminum base.

Frame on Al base for 9 g's loading					
Junction	Joining Method	Shear failure mode	Max allowable shear force (lbs)	Tensile failure mode	Max alloawable force (lbs)
Front/Back rails	20 * 3330	3330 sl	12000	3330 st	80400
Right/left rails	10 * 3330	3330 sh	27300	3330 st	40200
Total			**39300**		**120600**

9 g's forward loading condition				
Shear limit (lbs)	39300	Tensile limit (lbs)	120600
Shear force under 9 g's forward loading (lbs)	3690	Tensile force under 9 g's forward loading (in-lbs)	1691
Safety factor (Force)	11	Safety factor (Moment)	71

The stresses that the plate experiences as a result of loads applied to the entire system are shown below. As mentioned above, this portion of the analysis was done numerically. First we looked into the induced stresses as the entire experiment would slide under the 9 g's forward loading configurations. The simulation in figure 7 shows the safety factors resulting from this load.

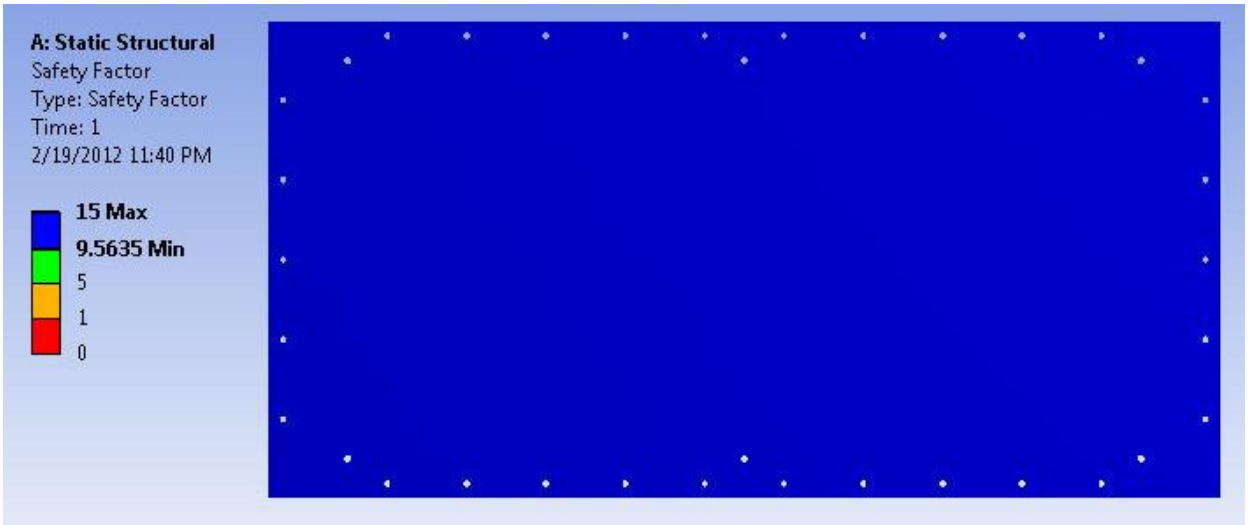

Figure A1.23. Safety factor simulation for the Aluminum base under the highest possible shear load

For the tensile case we had to assume that the reactions at each of the 6 bolt holes that keep the system attached to the aircraft would be equal. If the moment hinge is located at the edge of the experimental system, the average moment arm is 24 inches long. Based on that, the tension around each hole is 550 lbs. Figure 8 shows the safety factor calculation for this configuration. The stress concentration around each hole is quite low. It also should be taken into account than in reality, the stress would be concentrated around a larger area determined by the head of the bolt, hence there would be even higher safety factors. ANSYS however, applies the loads directly on the hole, which results in an artificial increase of the stresses.

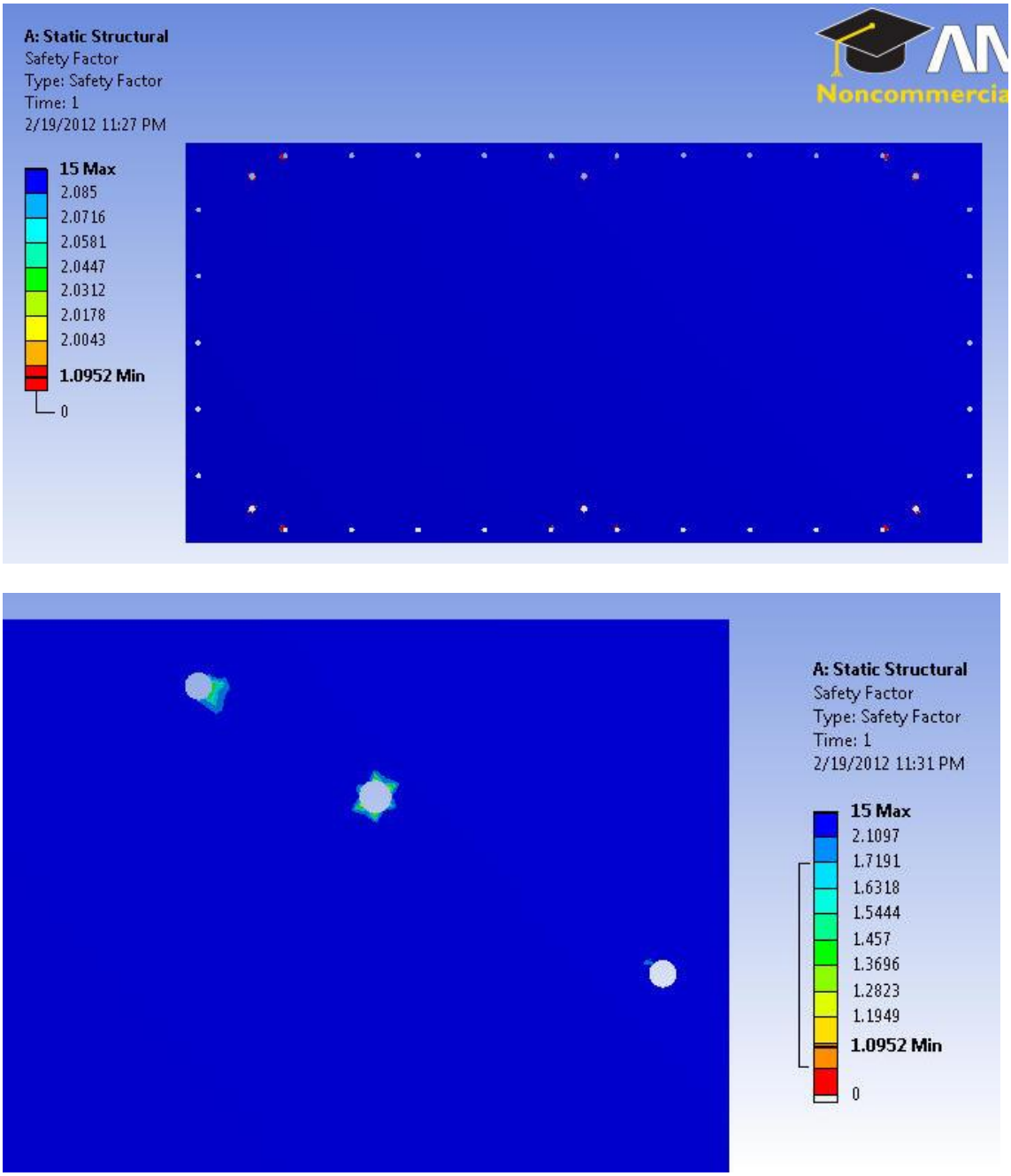

Figure A1.24. Safety factor calculation for the Aluminum base under the highest possible tensile load.

Load on Aircraft Floor

The entire system will be attached to the floor of the aircraft using the designated bolts and spacer configuration. The tolerances for the bolts are given in the ZGC-ICD document for the 727. Based on this we can calculate the safety factors. For the case of the tensile limit we assumed the moment induced by

the system as it would roll forward under the 9 g's specification would be opposed equally by all 6 bolts. Table 7 shows the safety factors calculated.

Table A1.21. Safety factor calculations for the aircraft floor attachment bolts

Shear limit (lbs)		15000		Tensile limit	12750
Force under 9 g's forward loading (lbs)		3690		Force under 9 g's forward loading (lbs)	1845
Safety factor (Shear)		4		Safety factor (Tension)	7

Chamber system

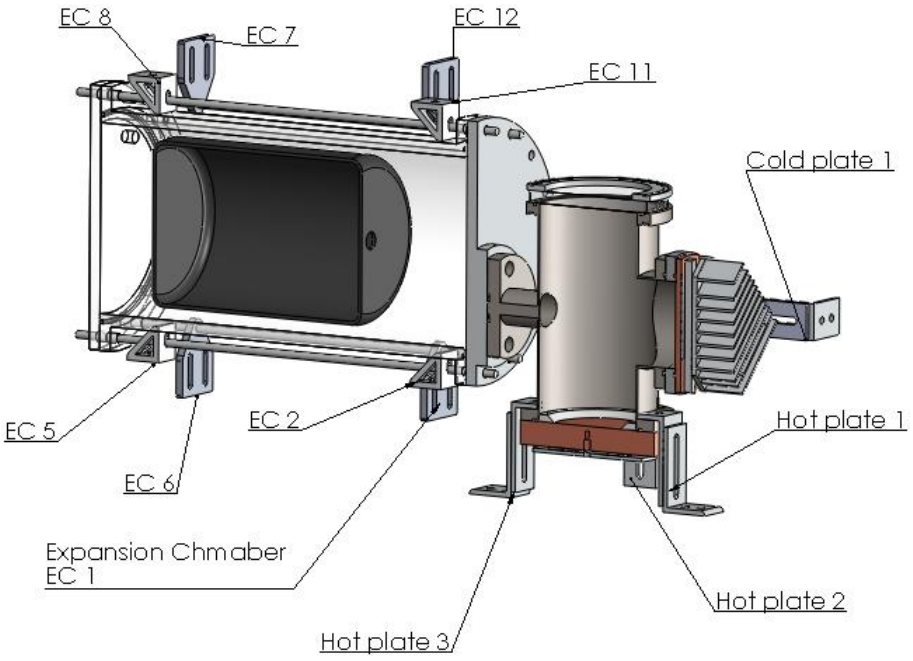

Figure A1.25. Sketch and nomenclature of chamber system joints

The chamber system is the most complex part to analyze given the different number of joints used. As costmary, the tables which outline the loading limit calculations will follow the nomenclature shown in figure 6. As mentioned before, we have assumed that all joints are equally loaded. Tables 6 through 8 will show the junctions tolerances and calculated safety factors.

Table A1.22. Chamber system tolerances and safety factors for the 9 g's forward load condition

Chamber system tolerances for forawrd-aft loads						
Junction		Joining Method	Shear failure mode	Max allowable shear force (lbs)	Moment failure mode	Max alloawable moment (in-lbs)
HP 1		1 * Slotted bracket system	SBs1	500	SBm1	200
HP 2		same	SBs2	600	SBm2	250
HP 3		same as HP 1	SBs1	500	SBm1	200
HP 4		same	SBs2	600	SBm2	250
CP1		same	SBs1	300	SBm1	200
CP2		same	SBs1	300	SBm1	200
EC1		1 * 2-slot plate	n/a	0	2SPm1	100
EC2		1 * 4332m	4332Ms1	500	4332Mm1	3000
EC3		same as EC1	n/a	0	2SPm1	100
EC4		same as EC1	n/a	0	2SPm1	100
EC5		same as EC2	4332Ms1	500	4332Mm1	3000
EC6		same as EC1	n/a	0	2SPm1	100
EC7		same as EC1	n/a	0	2SPm1	100
EC8		same as EC2	4332Ms1	500	4332Mm1	3000
EC9		same as EC1	n/a	0	2SPm1	100
EC10		same as EC1	n/a	0	2SPm1	100
EC11		same as EC2	4332Ms1	500	4332Mm1	3000
EC12		same as EC1	n/a	0	2SPm1	100
Total				**4800**		**14100**

9 g's forward loading condition						
Force limit (lbs)		4800		Moment limit (in-lbs)		14100
Force under 9 g's forward loading (lbs)		504		Moment under 9 g's forward loading (in-lbs)		4368
Safety factor (Force)		10		Safety factor (Moment)		3

Table A1.23. Chamber system tolerances and safety factors for the 6 g's aft load condition

Chamber system tolerances for aft loads						
Junction		Joining Method	Shear failure mode	Max allowable shear force (lbs)	Moment failure mode	Max alloawable moment (in-lbs)
HP 1		1 * Slotted bracket system	SBs1	500	SBm1	200
HP 2		same	SBs2	600	SBm2	250
HP 3		same as HP 1	SBs1	500	SBm1	200
HP 4		same	SBs2	600	SBm2	250
CP1		same	SBs1	300	SBm1	200
CP2		same	SBs1	300	SBm1	200
EC1		1 * 2-slot plate	n/a	100	2SPm1	600
EC3		same as EC1	n/a	100	2SPm1	600
EC4		same as EC1	n/a	100	2SPm1	600
EC6		same as EC1	n/a	100	2SPm1	600
EC7		same as EC1	n/a	100	2SPm1	600
EC9		same as EC1	n/a	100	2SPm1	600
EC10		same as EC1	n/a	100	2SPm1	600
EC12		same as EC1	n/a	100	2SPm1	600
Total				**3600**		**6100**

6 g's aft loading condition						
Force limit (lbs)		3600		Moment limit (in-lbs)		6100
Force under 3 g's aft loading (lbs)		168		Moment under 3 g's aft loading (in-lbs)		1456
Safety factor (Force)		21		Safety factor (Moment)		4

Table A1.24. Chamber system tolerances and safety factors for the 6 g's downward load condition

Chamber system tolerances for up-down loads						
Junction		Joining Method	Shear failure mode	Max allowable shear force (lbs)	Moment failure mode	Max alloawable moment (in-lbs)
HP 1		1 * Slotted bracket system	SBs1	400	SBm2	200
HP 2		same	SBs1	400	SBm2	200
HP 3		same	SBs1	400	SBm2	200
HP 4		same	SBs1	400	SBm2	200
CP1		same	SBs2	500	SBm1	250
CP2		same	SBs2	500	SBm1	250
EC1		1 * 2-slot plate	2SPs1	500	2SPm1	100
EC2		1 * 4332M	4332Mc	4000	4332Mm2	3000
EC3		same as EC1	2SPs1	500	2SPm1	100
EC4		same as EC1	2SPs1	500	2SPm1	100
EC5		same as EC2	4332Mc	4000	4332Mm2	3000
EC6		same as EC1	2SPs1	500	2SPm1	100
EC7		same as EC1	2SPs1	500	2SPm1	100
EC8		same as EC2	4332Mc	4000	4332Mm2	3000
EC9		same as EC1	2SPs1	500	2SPm1	100
EC10		same as EC1	2SPs1	500	2SPm1	100
EC11		same as EC2	4332Mc	4000	4332Mm2	3000
EC12		same as EC1	2SPs1	500	2SPm1	100
Total				**22600**		**14100**

Chamber system 6 g's downward loading condition						
Force limit (lbs)		22600		Moment limit (in-lbs)		14100
Force under 6 g's downward loading (lbs)		336		Moment under 6 g's downward loading (in-lbs)		5040
Safety factor (Force)		67		Safety factor (Moment)		3

*Also satisfies the 2 g's upward load condition

Table A1.25. Chamber system tolerances and safety factors for the 2 g's lateral load condition

Chamber system tolerances forlateral loads						
Junction		Joining Method	Shear failure mode	Max allowable shear force (lbs)	Moment failure mode	Max alloawable moment (in-lbs)
HP 1		1 * Slotted bracket system	SBs1	500	SBm2	250
HP 2		same	SBs1	400	SBm2	200
HP 3		same	SBs1	500	SBm2	250
HP 4		same	SBs1	400	SBm2	350
CP1		same	SBs1	400	SBm1	200
CP2		same	SBs1	400	SBm1	200
EC1		1 * 2-slot plate	2SPs2	1200	2SPm1	100
EC2		1 * 4332M	4332Ms1	600	4332Mm3	1000
EC3		same as EC1	2SPs2	1200	2SPm1	100
EC4		same as EC1	2SPs2	1200	2SPm1	100
EC5		same as EC2	4332Ms1	600	4332Mm3	1000
EC6		same as EC1	2SPs2	1200	2SPm1	100
EC7		same as EC1	2SPs2	1200	2SPm1	100
EC8		same as EC2	4332Ms1	600	4332Mm3	1000
EC9		same as EC1	2SPs2	1200	2SPm1	100
EC10		same as EC1	2SPs2	1200	2SPm1	100
EC11		same as EC2	4332Ms1	600	4332Mm3	1000
EC12		same as EC1	2SPs2	1200	2SPm1	100
Total				**14600**		**6250**

Chamber system 2 g's lateral loading condition						
Force limit (lbs)		14600		Moment limit (in-lbs)		6250
Force under 2 g's lateral loading (lbs)		112		Moment under 2 g's lateral loading (in-lbs)		700
Safety factor (Force)		130		Safety factor (Moment)		9

Vacuum Pump

In order to minimize the moment induced on the vertical beam junctions along the bottom section, some equipment was mounted directly on the bottom beams. Given the mass of the pump, it could only be efficiently mounted in such way. Hence the pump attachments have to be analyzed separately from other sections of the frame.

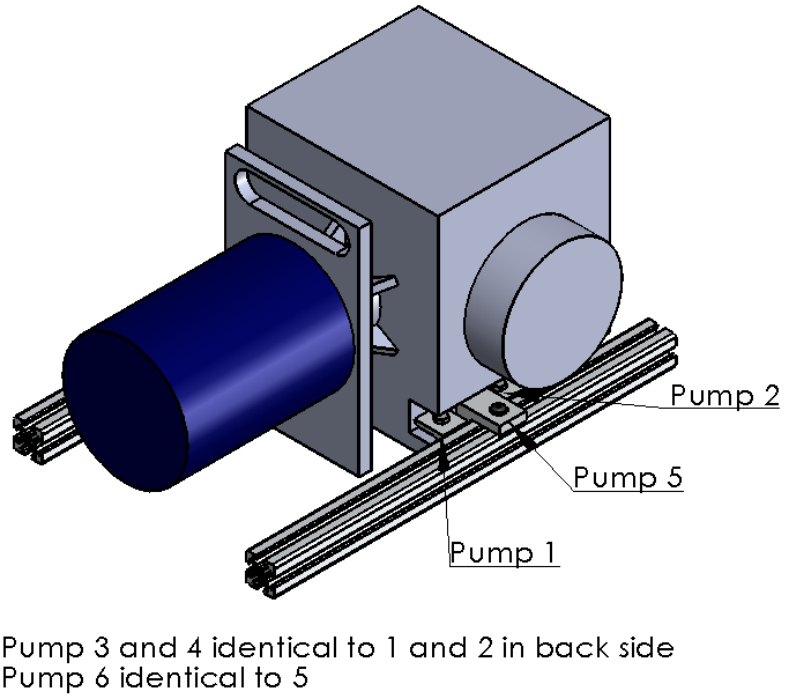

Figure A1.26. Sketch and nomenclature of pump joints

Table A1.26. Tolerances and safety factors of pump brackets for the 9 g's forward loading configuration

Pump bracket tolerances for forward-aft loads						
Junction		Joining Method	Shear failure mode	Max allowable shear force (lbs)	Moment failure mode	Max alloawable moment (in-lbs)
Pump 1		1 * 4302	4302s2	2700	4302m2	400
Pump 2		same	4301s2	2700	4302m2	400
Pump 3		same	4301s2	2700	4302m2	400
Pump 4		same	4301s2	2700	4302m2	400
Pump 5		1 * EPB	EPBs1	0	EPBm1	3100
Pump 6		same	EPBs1	0	EPBm1	3100
Total				**10800**		**7800**

Pump bracket 9 g's forward loading condition						
Force limit (lbs)		10800		Moment limit (in-lbs)		7800
Force under 9 g's forward loading (lbs)		630		Moment under 9 g's forward loading (in-lbs)		3780
Safety factor (Force)		17		Safety factor (Moment)		2

The pump is resting directly on the floor of the aircraft, so the downward load does not apply to the system.

Table A1.27. Tolerances and safety factors of pump brackets for the 2 g's lateral loading configuration

Pump bracket tolerances for lateral loadings						
Junction		Joining Method	Shear failure mode	Max allowable shear force (lbs)	Moment failure mode	Max alloawable moment (in-lbs)
Pump 1		1 * 4302	4302s1	600	4302m3h	800
Pump 2		same	4302s2	600	4302m3h	800
Pump 3		same	4302s2	600	4302m3h	800
Pump 4		same	4302s2	600	4302m3h	800
Pump 5		1 * EPB	EPBs1	0	EPBm1	0
Pump 6		same	EPBs1	0	EPBm1	0
Total				**2400**		**3200**

Pump bracket 2 g's lateral loading condition						
Force limit (lbs)		2400		Moment limit (in-lbs)		3200
Force under 2 g's lateral loading (lbs)		140		Moment under 2 g's lateral loading (in-lbs)		700
Safety factor (Force)		17		Safety factor (Moment)		5

Table A1.28. Tolerances and safety factors of pump brackets for the 2 g's upward loading configuration

Pump bracket tolerances for upward loading						
Junction		Joining Method	Shear failure mode	Max allowable shear force (lbs)	Moment failure mode	Max alloawable moment (in-lbs)
Pump 1		1 * 4302	4302s2	2700	4302m2	350
Pump 2		same	4302s2	2700	4302m2	350
Pump 3		same	4302s2	2700	4302m2	350
Pump 4		same	4302s2	2700	4302m2	350
Pump 5		1 * EPB	EPBs1	0	EPBm1	3100
Pump 6		same	EPBs1	0	EPBm1	3100
Total				**10800**		**7600**

Pump bracket 2 g's upward loading condition						
Force limit (lbs)		10800		Moment limit (in-lbs)		7600
Force under 2 g's upward loading (lbs)		140		Moment under 2 g's upward loading (in-lbs)		700
Safety factor (Force)		77		Safety factor (Moment)		11

Concave Mirror

The concave mirror is used as the collimating element in the system. A minor deviation from the ideal alignment would have severe negative effects on the image quality. Hence, the whole system must be extremely rigid, while still providing a certain level of mobility so that the optical alignment can be done. When each of the systems in the schlieren set up were designed, we aimed at having the smallest possible deformation, during the normal 2 g's operating cycle. Even though we will not analyze, and possibly not even record data while the aircraft is in the high g's portion of the flight path, we did not want to allow any of the critical components to constantly undergo deformation cycles. This is why safety factors associated with all optical equipment are considerably high. Figure 8 shows the bracketing labeling system and tables 12 through 14 display the tolerances and safety factors.

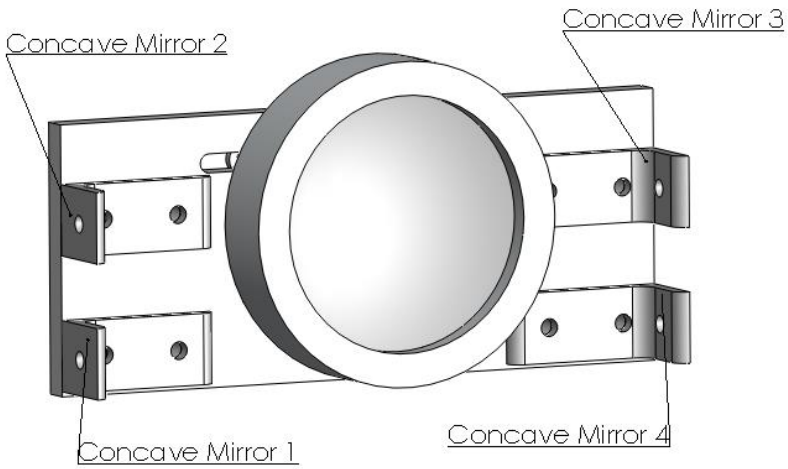

Figure A1.27. Concave mirror system drawing with joint labeling system

Table 29. Concave mirror system tolerances and safety factors for the 9 g's forward loading condition

Concave mirror along the forward-aft					
Junction	Joining Method	Shear failure mode	Max allowable shear force (lbs)	Moment failure mode	Max alloawable moment (in-lbs)
FM 1	1 * 4376	4302s2	2700	4302m1	420
FM 2	same	4302s2	2700	4302m1	420
FM 3	same	4302s2	2700	4302m1	420
FM 4	same	4302s2	2700	4302m1	420
Total			**10800**		**1680**

9 g's forward loading condition			
Force limit (lbs)	10800	Moment limit (in-lbs)	1680
Force under 9 g's forward loading (lbs)	59	Moment under 9 g's forward loading (in-lbs)	380
Safety factor (Force)	185	Safety factor (Moment)	4

The previous calculations automatically satisfy the 3 g's aft loading condition.

Table A1.30. Concave mirror system tolerances and safety factors for the 6 g's downward loading condition

Concave mirror along the up-down line					
Junction	Joining Method	Shear failure mode	Max allowable shear force (lbs)	Moment failure mode	Max alloawable moment (in-lbs)
CM 1	1 * 4376	4302s1	600	4302m3h	800
CM 2	same	4302s1	600	4302m3h	800
CM 3	same	4302s1	600	4302m3h	800
CM 4	same	4302s1	600	4302m3h	800
Total			**2400**		**3200**

6 g's downward loading condition				
Force limit (lbs)	2400	Moment limit (in-lbs)	3200
Force under 6 g's downward loading (lbs)	39	Moment under 6 g's downward loading (in lbs)	254
Safety factor (Force)	62	Safety factor (Moment)	13

The previous calculations automatically satisfy the 2 g's upward loading condition.

Table A1.31. Concave mirror system tolerances and safety factors for the 6 g's downward loading condition

Concave mirror along thelateral line						
Junction		Joining Method	Shear failure mode	Max allowable shear force (lbs)	Moment failure mode	Max alloawable moment (in-lbs)
CM 1		1 * 4376	4302s2	2700	4302m1	420
CM 2		same	4302s2	2700	4302m1	420
CM 3		same	4302s2	2700	4302m2	400
CM 4		same	4302s2	2700	4302m2	400
Total				**10800**		**1640**

2 g's lateral loading condition						
Force limit (lbs)		10800		Moment limit (in-lbs)		1640
Force under 2 g's lateral loading (lbs)		13		Moment under 2 g's lateral loading (in-lbs)		13
Safety factor (Force)		831		Safety factor (Moment)		126

Front Surface Mirror

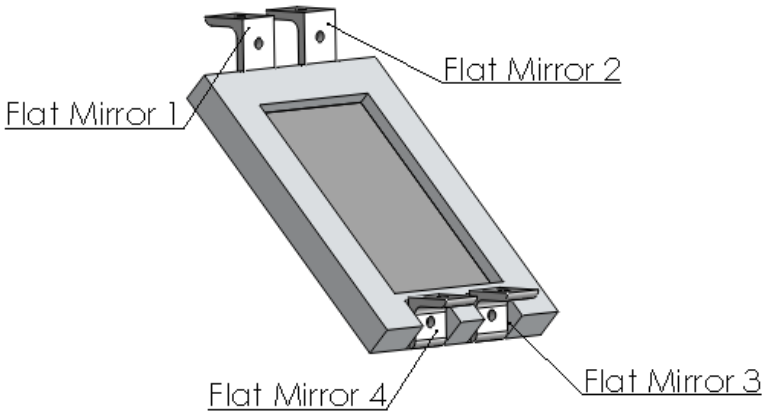

Figure A1.28. Front surface mirror system and joint labeling system

Table A1.32. Front surface mirror system tolerances and safety factors for the 9 g's forward loading condition

FSM tolerances for forward-aft loads						
Junction		Joining Method	Shear failure mode	Max allowable shear force (lbs)	Moment failure mode	Max alloawable moment (in-lbs)
FM 1		1 * 4376	4302s2	2700	4302m1	420
FM 2		same	4302s2	2700	4302m1	420
FM 3		1 * 4302	4302s2	2700	4302m2	400
FM 4		same	4302s2	2700	4302m2	400
Total				**10800**		**1640**

9 g's forward loading condition						
Force limit (lbs)		10800		Moment limit (in-lbs)		1640
Force under 9 g's forward loading (lbs)		45		Moment under 9 g's forward loading (in-lbs)		135
Safety factor (Force)		240		Safety factor (Moment)		12

Given that we have assumed the same tolerances values for the 4376 brackets as those for the 4302, the front surface mirror system will have the same tolerances along the forward-aft line and up-down line, hence, the forward 9 g's loading automatically satisfies the 3 g's aft, 6 g's down and 2 g's up loading conditions.

Table A1.33. Front surface mirror system tolerances and safety factors for the 2 g's lateral loading condition

FSM tolerances for lateral loads						
Junction		Joining Method	Shear failure mode	Max allowable shear force (lbs)	Moment failure mode	Max alloawable moment (in-lbs)
FM 1		1 * 4376	4302s2	600	4302m3h	800
FM 2		same	4302s2	600	4302m3h	800
FM 3		1 * 4302	4302s2	600	4302m3h	800
FM 4		same	4302s2	600	4302m3h	800
Total				**2400**		**3200**

FSM system 2 g's lateral loading condition						
Force limit (lbs)		2400		Moment limit (in-lbs)		3200
Force under 2 g's lateral loading (lbs)		10		Moment under 2 g's lateral loading (in-lbs)		30
Safety factor (Force)		240		Safety factor (Moment)		107

Clear covers

The structural analysis of the covers was done numerically assuming Plexyglass as the material of choice, even though it was later changed to the more resistant Lexan. This method was chosen for the covers because each numerical simulation would only involve one single part, rather than multiple parts and brackets as with most previous systems. Only two loads were analyzed for each cover: the highest normal load pulling the cover from the frame, and the highest in-plane load.

The covers are labeled as shown in figure with back cover opposite to front and left cover identical but opposite to right cover. In the bottom we have the Aluminum plate which we have already analyzed.

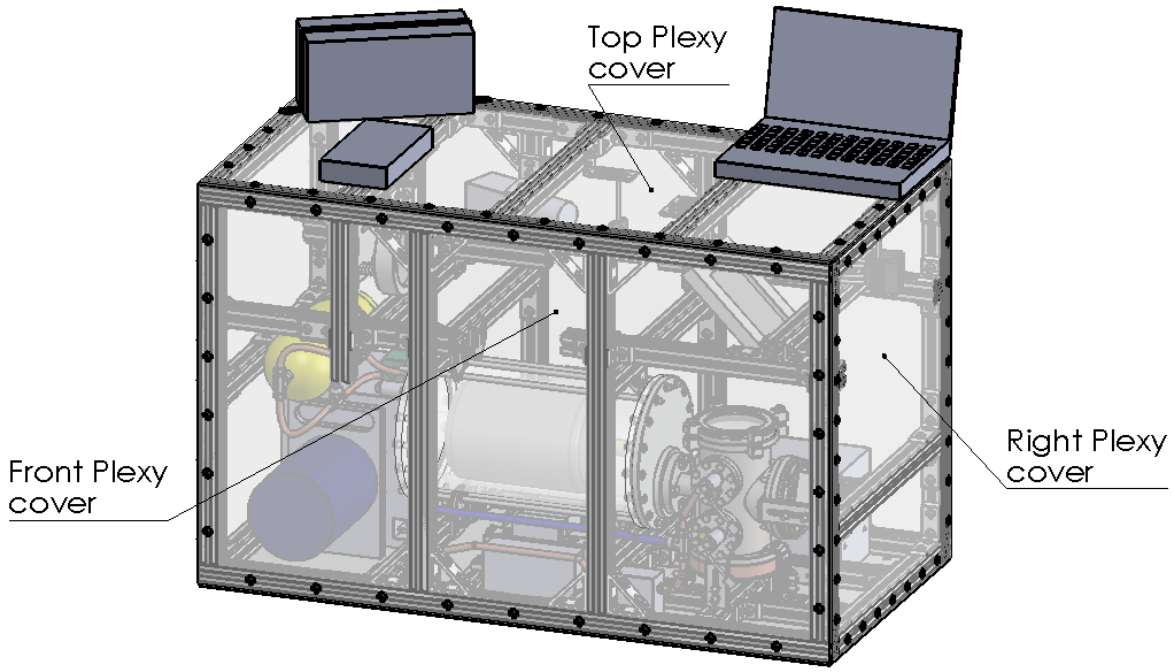

Figure A1.29. Assembly with covers

Table A1.34. Safety factors obtained assuming Plexyglass covers.

Part	Highest normal load	Safety factor	Highest in-plane load	Safety factor
Front/Back	2 G's	10	9 G's	60
Right/Left	9 G's	7	6 G's	450
Top	2 G's	19	9 G's	130

We ran these studies by applying the load, then increasing the safety factor until finding the value at which the part would fail. In reality these simulations are extremely conservative. We are considering the stresses will be concentrated in the hole itself, rather than being distributed by the bolt head more evenly over a bigger surface. However, given than Plexyglass is more brittle than Aluminum, the value reported in table 19 is the value at which the slightest failure was observed. Figure 13 show the procedure

followed. We will only include one study, right/left covers under the 9 g's forward spec. All other cases were performed in a similar fashion.

Model name: Right_left_plexy
Study name: SimulationXpress Study
Plot type: Factor of Safety Factor of Safety
Criterion : Max von Mises Stress
Red < FOS = 7 < Blue

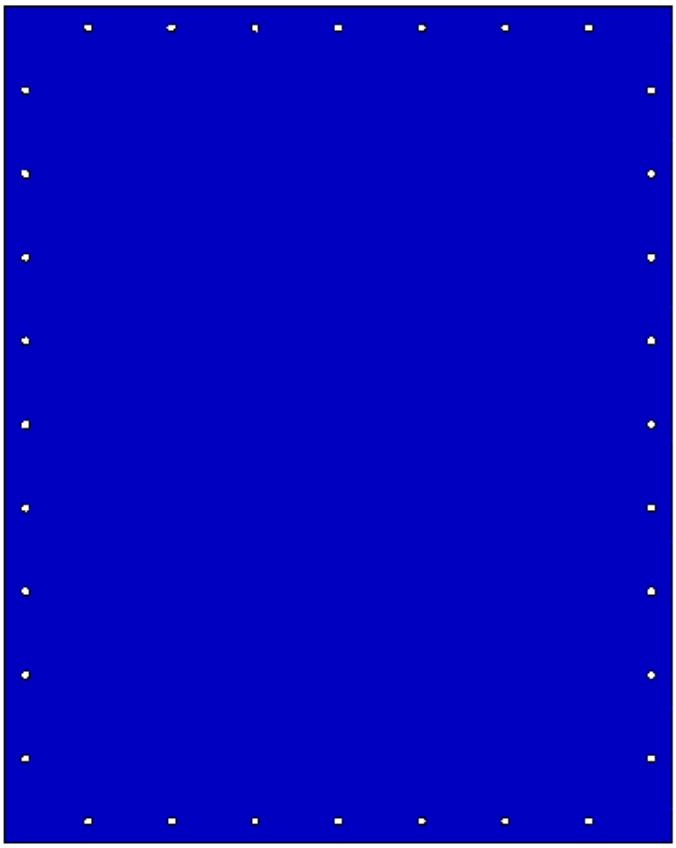

Model name: Right_left_plexy
Study name: SimulationXpress Study
Plot type: Factor of Safety Factor of Safety
Criterion : Max von Mises Stress
Red < FOS = 8 < Blue

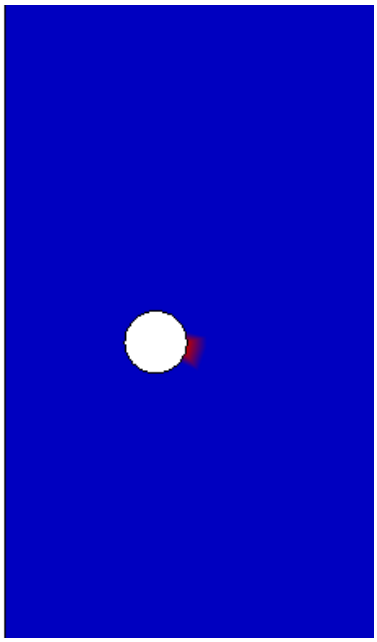

Figure A1.30. View of entire piece, with no section below safety factor 1 (top) and zoom of the first section with a safety factor below 1 (bottom). The highest safety factor without any failing portion determines the safety factor for the part under the given load.

Top Equipment

Three separate pieces of equipment will be placed on top of the frame itself: a scope, the MX-25 thickness gauge and the laptop computer used to collect data. A pull test has been performed on each of the equipment to ensure they can withstand the specified loads.

Scope

The scope is mounted to the frame by a combination of metal brackets and band clamps. The pull test was performed by hanging 50 lb weights from it (one or two, depending on the load configuration). A picture showing the scope attached with the weights hanging from it in the 9 g's forward configuration can be seen below. Similar tests were performed for all other configurations (except downwards)

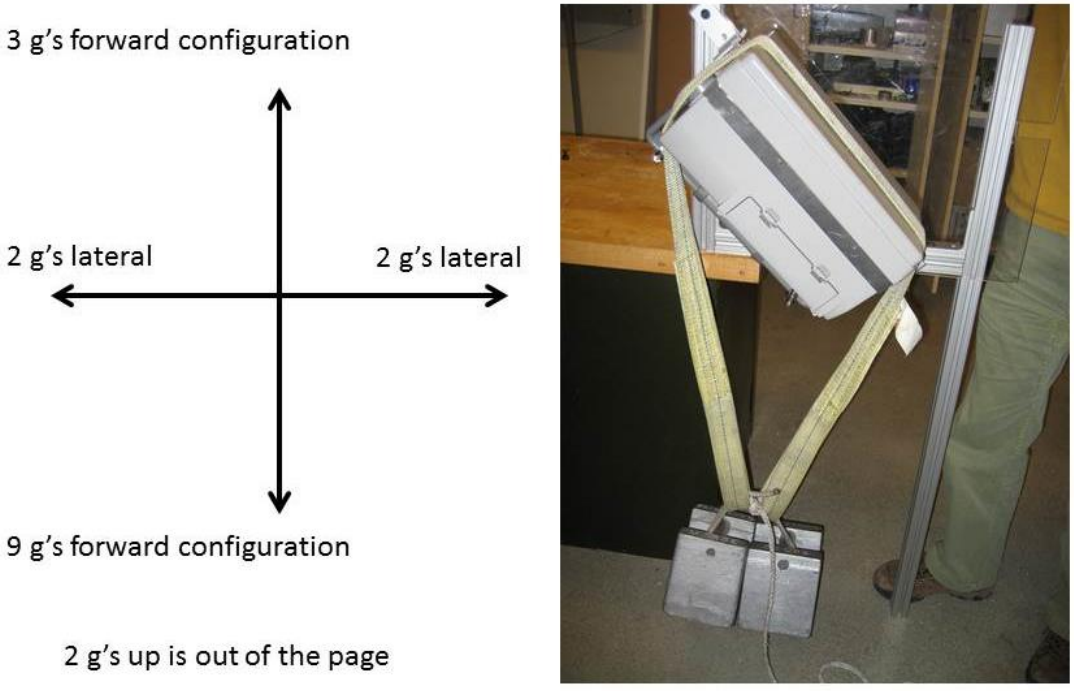

Figure A1.31. Scope mounted with loads equivalent to a 9 g forward acceleration being applied.

Equipment Pull-test Worksheet/Report Project: Film Evaporation Date: 4/5/12

Item Description:	Scope		
Manufacturer:	Agilent Technologies	Model No.:	DSO5054A
Dimensions (in.)[1]:	15" x 7.5" x 6.85"	Weight:	9 lbs
Gauge Description:	100 lb weights		
Manufacturer:	N/A	Model No.:	N/A
Serial No.:	N/A	NASA Tag:	N/A
Cal. Date:	N/A	Cal. Due:	N/A
Notes, comments:			
Case 1:	L.F.[2] 9g Dir. +X	**Case 2:**	L.F.[2] 3g Dir. -X
Target Load (lb):	81 lbs	Target Load (lb):	27 lbs
Max. load applied[3]:	100 lbs	Max. load applied[3]:	50 lbs
Hold Time:	1 min	Hold Time:	1 min
Inspector (sign.):		Inspector (sign.):	
Case 3:	L.F.[2] 2g Dir. +Y	**Case 4:**	L.F.[2] 2g Dir. -Y
Target Load (lb):	18 lbs	Target Load (lb):	18 lbs
Max. load applied[3]:	50 lbs	Max. load applied[3]:	50 lbs
Hold Time:	1 min	Hold Time:	1 min
Inspector (sign.):		Inspector (sign.):	
Case 5:	L.F.[2] 2g Dir. Up	**Case 6:**	L.F.[2] 6g Dir. Dn
Target Load (lb):	18 lbs	Target Load (lb):	N/A
Max. load applied[3]:	50 lbs	Max. load applied[3]:	
Hold Time:	1 min	Hold Time:	
Inspector (sign.):		Inspector (sign.):	

[1]Length x Width x Height
[2]Load Factor
[3]Optional

Inspector (print name): Juan Carlos Gonzalez (University of Washington)

This report is not valid unless accompanied by signature of inspector.

Signature of inspector certifies that the minimum load applied over the specified hold time is equal to or greater than the target load specified.

Loads must be applied at/through equipment Center of Gravity (CG), or corrected computationally to CG.

Include a sketch on a separate sheet to indicate coordinate axes employed and locations of force application.

Figure A1.32. Scope pull test sheet

Figure A1.33. Alternate scope mounting view.

Laptop PC.

A similar method was chosen to ensure the laptop could withstand the specified loads. The tests on the laptop were performed with it closed (take-off and landing configuration) as shown in figures 18 and 20. The laptop brackets include wing nuts, so that it can be opened in flight without need for tools. The pull tests on the laptop were done applying the minimum amount of force possible, while still complying with the loads, in order to prevent critical, somewhat weak parts like the screen, from

breaking. For this reason only in the 9 g's forward and 3 g's aft was the weight employed. In all other configurations, a force gauge was used to apply the load.

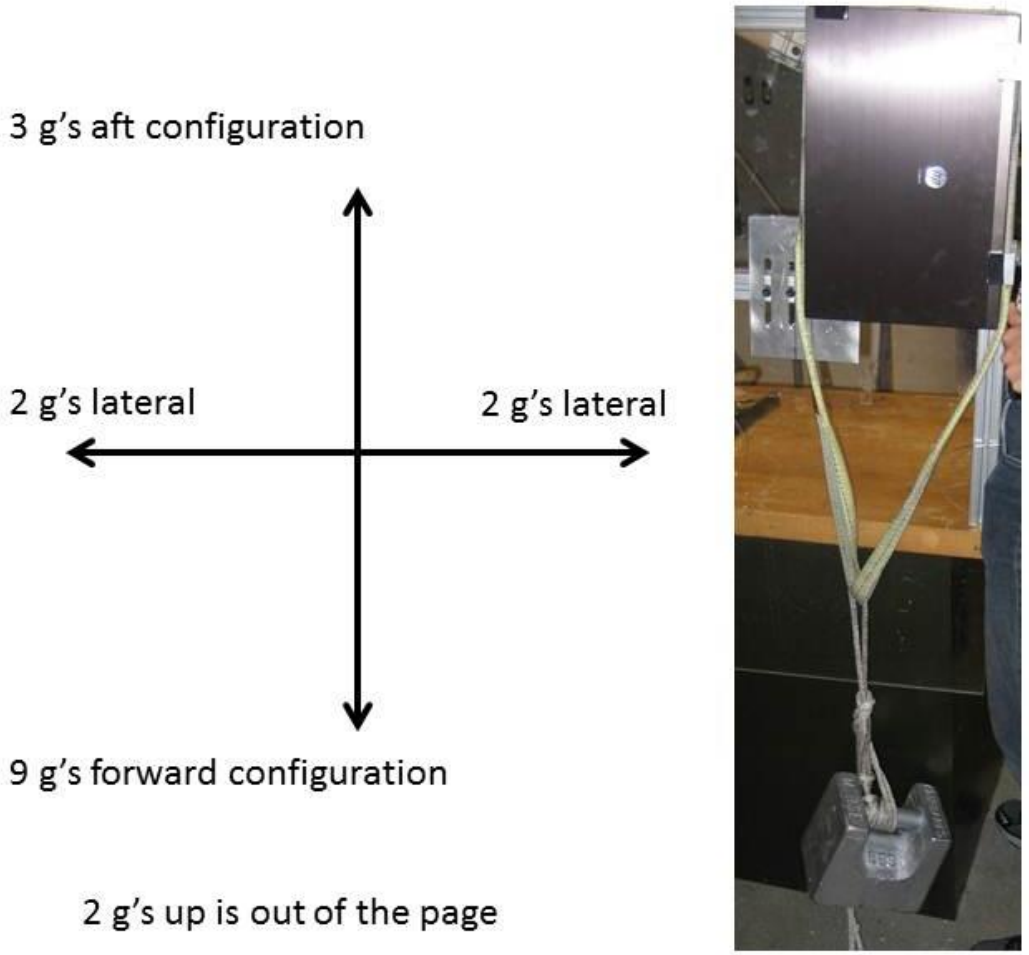

Figure A1.34. Laptop mounted with loads equivalent to that of a 9 g forward acceleration being applied

Equipment Pull-test Worksheet/Report Project: Film Evaporation Date: 4/5/12

Item Description:	Laptop		
Manufacturer:	HP	Model No.:	4525S
Dimensions (in.)[1]:	1.09" x 14.6" x 9.83"	Weight:	5.55 lbs
Gauge Description:	50 lb weights		
Manufacturer:	N/A	Model No.:	N/A
Serial No.:	N/A	NASA Tag:	N/A
Cal. Date:	N/A	Cal. Due:	N/A
Notes, comments:			
Case 1:	L.F.[2] 9g Dir. +X	**Case 2:**	L.F.[2] 3g Dir. -X
Target Load (lb):	50 lbs	Target Load (lb):	16.65 lbs
Max. load applied[3]:	50 lbs	Max. load applied[3]:	50 lbs
Hold Time:	1 min	Hold Time:	1 min
Inspector (sign.):		Inspector (sign.):	
Case 3:	L.F.[2] 2g Dir. +Y	**Case 4:**	L.F.[2] 2g Dir. -Y
Target Load (lb):		Target Load (lb):	
Max. load applied[3]:		Max. load applied[3]:	
Hold Time:		Hold Time:	
Inspector (sign.):		Inspector (sign.):	
Case 5:	L.F.[2] 2g Dir. Up	**Case 6:**	L.F.[2] 6g Dir. Dn
Target Load (lb):		Target Load (lb):	
Max. load applied[3]:		Max. load applied[3]:	
Hold Time:		Hold Time:	
Inspector (sign.):		Inspector (sign.):	

[1]Length x Width x Height
[2]Load Factor
[3]Optional

Inspector (print name): Juan Carlos Gonzalez (University of Washington)

This report is not valid unless accompanied by signature of inspector.

Signature of inspector certifies that the minimum load applied over the specified hold time is equal to or greater than the target load specified.

Loads must be applied at/through equipment Center of Gravity (CG), or corrected computationally to CG.

Include a sketch on a separate sheet to indicate coordinate axes employed and locations of force application.

Equipment Pull-test Worksheet/Report Project: Film Evaporation Date: 4/5/12

Item Description:	Laptop		
Manufacturer:	HP	Model No.:	4525S
Dimensions (in.)[1]:	1.09" x 14.6" x 9.83"	Weight:	5.55 lbs
Gauge Description:	Pull force gauge		
Manufacturer:	Salter	Model No.:	235 6S
Serial No.:	N/A	NASA Tag:	N/A
Cal. Date:	4/5/12 (checked against known weights)	Cal. Due:	N/A
Notes, comments:			
Case 1:	L.F.[2] 9g Dir. +X	**Case 2:**	L.F.[2] 3g Dir. -X
Target Load (lb):		Target Load (lb):	
Max. load applied[3]:		Max. load applied[3]:	
Hold Time:		Hold Time:	
Inspector (sign.):		Inspector (sign.):	
Case 3:	L.F.[2] 2g Dir. +Y	**Case 4:**	L.F.[2] 2g Dir. -Y
Target Load (lb):	11 lbs	Target Load (lb):	11 lbs
Max. load applied[3]:	11 lbs	Max. load applied[3]:	11 lbs
Hold Time:	1 min	Hold Time:	1 min
Inspector (sign.):		Inspector (sign.):	
Case 5:	L.F.[2] 2g Dir. Up	**Case 6:**	L.F.[2] 6g Dir. Dn
Target Load (lb):	11 lbs	Target Load (lb):	N/A
Max. load applied[3]:	11 lbs	Max. load applied[3]:	
Hold Time:	1 min	Hold Time:	
Inspector (sign.):		Inspector (sign.):	

[1]Length x Width x Height
[2]Load Factor
[3]Optional

Inspector (print name): Juan Carlos Gonzalez (University of Washington)

This report is not valid unless accompanied by signature of inspector.

Signature of inspector certifies that the minimum load applied over the specified hold time is equal to or greater than the target load specified.

Loads must be applied at/through equipment Center of Gravity (CG), or corrected computationally to CG.

Include a sketch on a separate sheet to indicate coordinate axes employed and locations of force application.

Figure A1.35. Laptop pull test sheets

Figure A1.36. Close-up of the laptop mounts.

Thickness Gauge

The thickness gauge is the smallest, lightest and easiest top equipment to mount. Loads were applied with a force gauge in all configurations except downwards, as shown in figure 21.

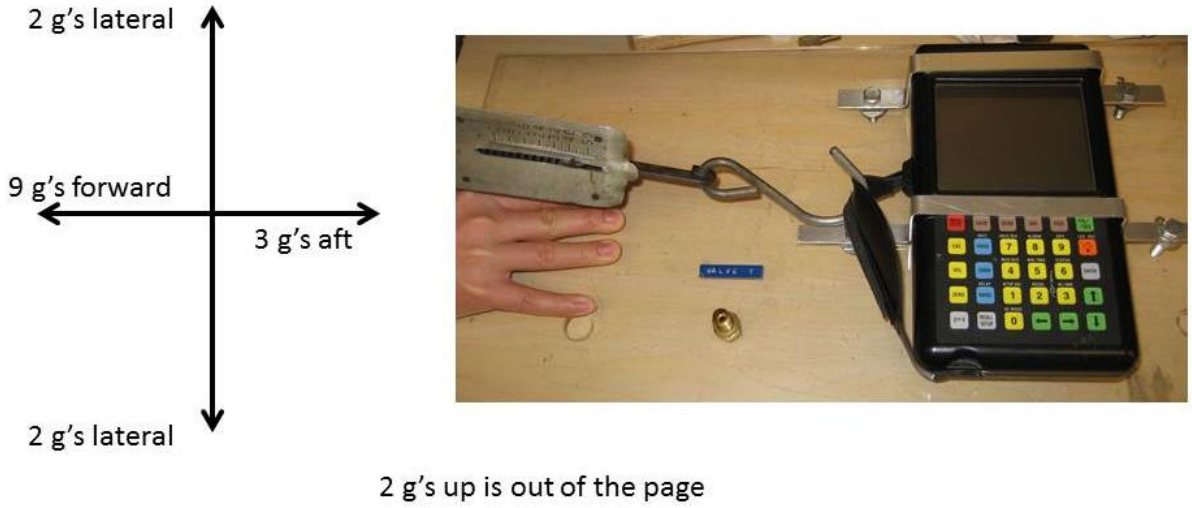

Figure A1.37. Thickness gauge with a load equivalent to a 9 g forward acceleration being applied

Equipment Pull-test Worksheet/Report Project: Film Evaporation Date: 4/5/12

Item Description:	Thickness Gauge		
Manufacturer:	Panametrics	Model No.:	MX 25
Dimensions (in.)[1]:	5.5" x 9.5" x 1.75"	Weight:	2.1 lbs
Gauge Description:	Pull force gauge		
Manufacturer:	John Chatillon	Model No.:	34 H
Serial No.:	N/A	NASA Tag:	N/A
Cal. Date:	4/5/12 (checked against known weights)	Cal. Due:	N/A
Notes, comments:			
Case 1:	L.F.[2] 9g Dir. +X	**Case 2:**	L.F.[2] 3g Dir. -X
Target Load (lb):	20 lbs	Target Load (lb):	7 lbs
Max. load applied[3]:	40 lbs	Max. load applied[3]:	16 lbs
Hold Time:	5 sec	Hold Time:	30 sec
Inspector (sign.):		Inspector (sign.):	
Case 3:	L.F.[2] 2g Dir. +Y	**Case 4:**	L.F.[2] 2g Dir. -Y
Target Load (lb):	5 lbs	Target Load (lb):	5 lbs
Max. load applied[3]:	16 lbs	Max. load applied[3]:	16 lbs
Hold Time:	30 ~~min~~ sec	Hold Time:	30 sec
Inspector (sign.):		Inspector (sign.):	
Case 5:	L.F.[2] 2g Dir. Up	**Case 6:**	L.F.[2] 6g Dir. Dn
Target Load (lb):	5 lbs	Target Load (lb):	N/A
Max. load applied[3]:	16 lbs	Max. load applied[3]:	
Hold Time:	30 sec	Hold Time:	
Inspector (sign.):		Inspector (sign.):	

[1]Length x Width x Height
[2]Load Factor
[3]Optional

Inspector (print name): Juan Carlos Gonzalez (University of Washington)

This report is not valid unless accompanied by signature of inspector.

Signature of inspector certifies that the minimum load applied over the specified hold time is equal to or greater than the target load specified.

Loads must be applied at/through equipment Center of Gravity (CG), or corrected computationally to CG.

Include a sketch on a separate sheet to indicate coordinate axes employed and locations of force application.

Figure A1.38. Thickness gauge pull test sheet.

Appendix B. Dichloromethane MSDS

ACC# 14930

Section 1 - Chemical Product and Company Identification

MSDS Name: Dichloromethane
Catalog Numbers: AC113460000, AC113460010, AC113460025, AC113460050, AC113460051, AC113460100, AC113460250, AC124050000, AC124050010, AC124050025, AC124050050, AC124050100, AC124050250, AC167770000, AC167770025, AC167775000, AC268330000, AC268330010, AC268330025, AC326600000, AC326600010, AC326600025, AC326760000, AC326760010, AC326760025, AC326850000, AC326850010, AC326850025, AC326851000, AC326852500, AC327870000, AC327870010, AC348460000, AC348460010, AC348460025, AC348461000, AC348465000, AC354800000, AC354800025, AC364230000, AC364230010, AC364230025, AC379130000, AC379130010, AC379130025, AC383780000, AC383780010, AC383780025, AC383780050, AC383780250, AC390700000, AC390700010, AC390700025, AC406910000, AC406910010, AC406910040, AC406910200, AC406920000, AC406930000, AC406935000, AC61030019, AC61030050, AC61030050, AC61030115, AC61030115, AC61030200, 32660-0040, 40692-0010, 40692-0040, 40692-5000, 61005-0040, 61016-0040, 61030-0010, 61030-1000, 61093-1000, BP1186-4, BP1186POP-200, BP1186POP20, BP1186SS-19, BP1186SS-200, BP1186SS-28, BP1186SS-50, BP2608-100, D138-1, D138-4, D138SK-4, D142-4, D142RS-115, D142RS-19, D142RS-50, D142RS200, D142RS28, D142SS-115, D142SS-200, D142SS-28, D142SS-50, D143-1, D143-4, D143-4LC, D143N2-19, D143POP28, D143RS-19, D143RS-200, D143RS-28, D143RS115, D143RS50, D143SK-1, D143SK-4, D143SK4LC, D143SS-115, D143SS-19, D143SS-200, D143SS-28, D143SS-50, D149RS-19, D149RS-200, D149RS-50, D150-1, D150-4, D1504LC, D150SK-1, D150SK-4, D151-1, D151-4, D151-4LC, D151RS-115, D151RS-19, D151RS-200, D151RS-28, D151RS-50, D151SK-4, D151SS-115, D151SS-19, D151SS-200, D151SS-28, D151SS-50, D154-4, D1544LC, D158-4, D35-1, D35-4, D37-1, D37-20, D37-200, D37-4, D37-500, D37FB-115, D37FB-19, D37FB-200, D37FB-50, D37POP19, D37POPB-200, D37POPB-50, D37RB-115, D37RB-19, D37RB-200, D37RB-50, D37RS-115, D37RS-200, D37RS-28, D37RS-50, D37RS19, D37SK-4, D37SS-115, D37SS-200, D37SS-28, D37SS-50, D37SS1350, NC9026865, NC9195811, NC9206961, NC9445086, NC9520903, NC9734652
Synonyms: Methylene chloride; Methane dichloride; Methylene bichloride; Methylene dichloride; Dichloromethane; DCM.
Company Identification:

Fisher Scientific
1 Reagent Lane
Fair Lawn, NJ 07410

For information, call: 201-796-7100
Emergency Number: 201-796-7100
For CHEMTREC assistance, call: 800-424-9300
For International CHEMTREC assistance, call: 703-527-3887

Section 2 - Composition, Information on Ingredients

CAS#	Chemical Name	Percent	EINECS/ELINCS
75-09-2	Methylene chloride	>99.5	200-838-9

Section 3 - Hazards Identification

EMERGENCY OVERVIEW

Appearance: colorless liquid.
Warning! Methylene chloride is metabolically converted to carbon monoxide after systemic absorption, which yields increased concentrations of carboxyhemoglobin in the blood. Harmful if swallowed. Causes eye, skin, and respiratory tract irritation. May be harmful if inhaled. Potential cancer hazard. This substance has caused adverse reproductive and fetal effects in animals. May cause central nervous system effects. May cause kidney damage.
Target Organs: Blood, central nervous system.

Potential Health Effects

Eye: Contact with eyes may cause severe irritation, and possible eye burns.
Skin: May be absorbed through the skin. Causes irritation with burning pain, itching, and redness. Prolonged exposure may result in skin burns.
Ingestion: Causes gastrointestinal irritation with nausea, vomiting and diarrhea. May cause kidney damage. May cause central nervous system depression, characterized by excitement, followed by headache, dizziness, drowsiness, and nausea. Advanced stages may cause collapse, unconsciousness, coma and possible death due to respiratory failure. May cause carboxyhemoglobinemia.
Inhalation: Inhalation of high concentrations may cause central nervous system effects characterized by nausea, headache, dizziness, unconsciousness and coma. Causes respiratory tract irritation. May cause narcotic effects in high concentration. Vapors may cause dizziness or suffocation. May cause blood changes. Overexposure may cause an increase in carboxyhemoglobin levels in the blood. Can produce delayed pulmonary edema. Because of its high volatility, airborne concentrations of methylene chloride can accumulate in poorly ventilated areas. Odor is a poor indicator of possibly dangerous air concentrations of methylene chloride.
Chronic: Possible cancer hazard based on tests with laboratory animals. Prolonged or repeated skin contact may cause dermatitis. May cause reproductive and fetal effects. Laboratory experiments have resulted in mutagenic effects. Chronic exposure may cause lung, liver, and pancreatic tumors. May cause conjunctivitis and/or corneal burns.

Section 4 - First Aid Measures

Eyes: In case of contact, immediately flush eyes with plenty of water for a t least 15 minutes. Get medical aid.
Skin: In case of contact, flush skin with plenty of water. Remove contaminated clothing and shoes. Get medical aid if irritation develops and persists. Wash clothing before reuse.
Ingestion: If swallowed, do not induce vomiting unless directed to do so by medical personnel. Never give anything by mouth to an unconscious person. Get medical aid.
Inhalation: If inhaled, remove to fresh air. If not breathing, give artificial respiration. If breathing is difficult, give oxygen. Get medical aid.
Notes to Physician: Treat symptomatically and supportively.

Section 5 - Fire Fighting Measures

General Information: As in any fire, wear a self-contained breathing apparatus in pressure-demand, MSHA/NIOSH (approved or equivalent), and full protective gear. Use

water spray to keep fire-exposed containers cool. No flash point in conventional closed tester, but forms flammable vapor-air mixtures in larger volumes and may be an explosion hazard in a confined space.
Extinguishing Media: Use water spray, dry chemical, carbon dioxide, or appropriate foam.
Flash Point: Not applicable.
Autoignition Temperature: 556 deg C (1,032.80 deg F)
Explosion Limits, Lower:13 vol %
Upper: 23 vol %
NFPA Rating: (estimated) Health: 2; Flammability: 1; Instability: 0

Section 6 - Accidental Release Measures

General Information: Use proper personal protective equipment as indicated in Section 8.
Spills/Leaks: Absorb spill with inert material (e.g. vermiculite, sand or earth), then place in suitable container. Avoid runoff into storm sewers and ditches which lead to waterways. Clean up spills immediately, observing precautions in the Protective Equipment section. Remove all sources of ignition. Provide ventilation.

Section 7 - Handling and Storage

Handling: Wash thoroughly after handling. Remove contaminated clothing and wash before reuse. Avoid contact with eyes, skin, and clothing. Keep container tightly closed. Keep away from heat, sparks and flame. Use only with adequate ventilation. Avoid breathing vapor or mist.
Storage: Store in a tightly closed container. Keep from contact with oxidizing materials. Store in a cool, dry, well-ventilated area away from incompatible substances. Store below 40°C. Keep away from active metals.

Section 8 - Exposure Controls, Personal Protection

Engineering Controls: Facilities storing or utilizing this material should be equipped with an eyewash facility and a safety shower. Use adequate general or local exhaust ventilation to keep airborne concentrations below the permissible exposure limits.
Exposure Limits

Chemical Name	ACGIH	NIOSH	OSHA - Final PELs
Methylene chloride	50 ppm TWA	2300 ppm IDLH	25 ppm TWA; 12.5 ppm Action Level; 25 ppm TWA; 125 ppm STEL (15 min, Cancer, cardiac effects , central nervous system effects, liver effects, and skin and eye irritation - See 29 CFR 1910.1052)

OSHA Vacated PELs: Methylene chloride: 500 ppm TWA
Personal Protective Equipment
Eyes: Wear chemical splash goggles.
Skin: Viton gloves are recommended.

Clothing: Wear appropriate protective clothing to prevent skin exposure.
Respirators: A respiratory protection program that meets OSHA's 29 CFR 1910.134 and ANSI Z88.2 requirements or European Standard EN 149 must be followed whenever workplace conditions warrant respirator use.

Section 9 - Physical and Chemical Properties

Physical State: Liquid
Appearance: colorless
Odor: ethereal odor - chloroform-like
pH: Not available.
Vapor Pressure: 350 mm Hg @ 20 deg C
Vapor Density: 2.93 (Air=1)
Evaporation Rate: Not available.
Viscosity: Not available.
Boiling Point: 40 deg C
Freezing/Melting Point:-97 deg C
Decomposition Temperature: Not available.
Solubility: Slightly soluble.
Specific Gravity/Density:1.33 (Water=1)
Molecular Formula:CH2Cl2
Molecular Weight:84.93

Section 10 - Stability and Reactivity

Chemical Stability: Stable at room temperature in closed containers under normal storage and handling conditions. May form explosive mixtures in atmospheres having high oxygen content.
Conditions to Avoid: Excess heat, attacks some plastics, rubber, and coatings, confined spaces, When no water is present, dichloromethane is not corrosive to metals. At high temperatures and in the presence of water (causing slow decomposition forming HCl), corrosion of iron, some stainless steels, copper and aluminum can occur..
Incompatibilities with Other Materials: Strong oxidizing agents, strong bases, chemically active metals.
Hazardous Decomposition Products: Hydrogen chloride, phosgene, carbon monoxide, carbon dioxide.
Hazardous Polymerization: Will not occur.

Section 11 - Toxicological Information

RTECS#:
CAS# 75-09-2: PA8050000
LD50/LC50:
CAS# 75-09-2:
Draize test, rabbit, eye: 162 mg Moderate;
Draize test, rabbit, eye: 10 mg Mild;
Draize test, rabbit, eye: 500 mg/24H Mild;
Draize test, rabbit, skin: 810 mg/24H Severe;

Draize test, rabbit, skin: 100 mg/24H Moderate;
Inhalation, mouse: LC50 = 14400 ppm/7H;
Inhalation, mouse: LC50 = 49100 mg/m3/6H;
Inhalation, mouse: LC50 = 54000 mg/m3/2H;
Inhalation, mouse: LC50 = 56220 mg/m3/7H;
Inhalation, rat: LC50 = 52 gm/m3;
Inhalation, rat: LC50 = 76000 mg/m3/4H;
Inhalation, rat: LC50 =

Carcinogenicity:

CAS# 75-09-2:

- **ACGIH:** A3 - Confirmed Animal Carcinogen with Unknown Relevance to Humans
- **California:** carcinogen, initial date 4/1/88
- **NTP:** Suspect carcinogen
- **IARC:** Group 2B carcinogen

Epidemiology: There are few reports of injury despite widespread use of dichloromethane (ACGIH, 1991). Solvent abuse has led to death (Harbison, 1998).
Teratogenicity: Inhalation, rat: TCLo = 4500 ppm/24H (female 1-17 day(s) after conception) Effects on Newborn - behavioral.; Inhalation, rat: TCLo = 1250 ppm/7H (female 6-15 day(s) after conception) Specific Developmental Abnormalities - musculoskeletal system and urogenital system.
Reproductive Effects: Adverse reproductive effects have occurred in experimental animals.
Mutagenicity: DNA inhibition: Human, Fibroblast = 5000 ppm/1H (Continuous).; Morphological transformation: Rat, Embryo = 160 umol/L.; DNA damage: Oral, rat = 1275 mg/kg.; Inhalation, mouse: TCLo = 2000 ppm/5H/2Y-C (Tumorigenic - Carcinogenic by RTECS criteria--Lungs, Thorax, or Respiration - Tumors).
Neurotoxicity: The neurotoxicity is thought to be due to a direct nonspecific CNS depressant action of dichloromethane and to indirect effects of carbon monoxide. Dichloromethane may exert acute effects on the nervous system by mechanisms related to its lipophilicity.
Other Studies:

Section 12 - Ecological Information

Ecotoxicity: Fish: Bluegill/Sunfish: 230mg/L; 24H; StaticFish: Fathead Minnow: 196mg/L; 96H; This chemical has a moderate potential to affect some aquatic organisms. It is resistant to biodegradation, and has a low potential to persist in the aquatic environment. 96-hr. EC50 (loss of equilibrium); Fathead minnow: 99mg/L; 96-hr. EC10: 66.3 mg/L. Bluegill sunfish: 96-hr. LC50=220 mg/L; Water flea: 24-hr. LC50=2270 mg/L; No observed effect level:1550 mg/L.
Environmental: Terrestrial: Expected to evaporate from near surface soil into the atmosphere; expected to leach. Aquatic: Primarily lost by evaporation to the atmosphere which should take several hours depending on wind and mixing conditions. Atmospheric: Will degrade by reaction with hydroxyl radicals with a half life of several months. . Dichloromethane is reported to completely biodegrade under aerobic conditions with sewage seed or activated sludge between 6 hours to 7 days. Not expected to bioconcentrate due to its low octanol/water coefficient.
Physical: No information available.
Other: No information available.

Section 13 - Disposal Considerations

Chemical waste generators must determine whether a discarded chemical is classified as a hazardous waste. US EPA guidelines for the classification determination are listed in 40 CFR Parts 261.3. Additionally, waste generators must consult state and local hazardous waste regulations to ensure complete and accurate classification.
RCRA P-Series: None listed.
RCRA U-Series:
CAS# 75-09-2: waste number U080.

Section 14 - Transport Information

	US DOT	Canada TDG
Shipping Name:	DICHLOROMETHANE	DICHLOROMETHANE
Hazard Class:	6.1	6.1
UN Number:	UN1593	UN1593
Packing Group:	III	III

Section 15 - Regulatory Information

US FEDERAL

TSCA
CAS# 75-09-2 is listed on the TSCA inventory.
Health & Safety Reporting List
CAS# 75-09-2: Effective 10/4/82, Sunset 10/4/92
Chemical Test Rules
None of the chemicals in this product are under a Chemical Test Rule.
Section 12b
CAS# 75-09-2: Section 4, 0.1 % de minimus concentration
TSCA Significant New Use Rule
None of the chemicals in this material have a SNUR under TSCA.
CERCLA Hazardous Substances and corresponding RQs
CAS# 75-09-2: 1000 lb final RQ; 454 kg final RQ
SARA Section 302 Extremely Hazardous Substances
None of the chemicals in this product have a TPQ.
SARA Codes
CAS # 75-09-2: immediate, delayed.
Section 313
This material contains Methylene chloride (CAS# 75-09-2, >99.5%),which is subject to the reporting requirements of Section 313 of SARA Title III and 40 CFR Part 373.
Clean Air Act:
CAS# 75-09-2 is listed as a hazardous air pollutant (HAP).
This material does not contain any Class 1 Ozone depletors.
This material does not contain any Class 2 Ozone depletors.
Clean Water Act:
None of the chemicals in this product are listed as Hazardous Substances under the CWA. CAS# 75-09-2 is listed as a Priority Pollutant under the Clean Water Act. CAS#

75-09-2 is listed as a Toxic Pollutant under the Clean Water Act.

OSHA:

None of the chemicals in this product are considered highly hazardous by OSHA.

STATE

CAS# 75-09-2 can be found on the following state right to know lists: California, New Jersey, Pennsylvania, Minnesota, Massachusetts.

California Prop 65

The following statement(s) is(are) made in order to comply with the California Safe Drinking Water Act:

WARNING: This product contains Methylene chloride, a chemical known to the state of California to cause cancer.

California No Significant Risk Level: CAS# 75-09-2: 200 æg/day NSRL (inhalation); 50 æg/day NSRL

European/International Regulations

European Labeling in Accordance with EC Directives

Hazard Symbols:

XN

Risk Phrases:

R 40 Limited evidence of a carcinogenic effect.

Safety Phrases:

S 23 Do not inhale gas/fumes/vapour/spray.

S 24/25 Avoid contact with skin and eyes.

S 36/37 Wear suitable protective clothing and gloves.

WGK (Water Danger/Protection)

CAS# 75-09-2: 2

Canada - DSL/NDSL

CAS# 75-09-2 is listed on Canada's DSL List.

Canada - WHMIS

This product has a WHMIS classification of D2A.

This product has been classified in accordance with the hazard criteria of the Controlled Products Regulations and the MSDS contains all of the information required by those regulations.

Canadian Ingredient Disclosure List

CAS# 75-09-2 is listed on the Canadian Ingredient Disclosure List.

Section 16 - Additional Information

MSDS Creation Date: 4/20/1999

Revision #10 Date: 9/30/2008

Appendix C. Hydrostatic Tests Documentation

Test Chamber Hydrostatic test sheet.

The test chamber was submitted to a hydrostatic test. Given that the chamber is an expensive and essential part of the experiment, the test was not done until failure, but rather, until a level of pressure was reached that would result in compliant safety factors.

A. The test was done by filling the chamber with colored water, attaching in to a standard tap water outlet in order to pressurize it. The copper plate used as an evaporation surface was removed, but the optical port, the condensing copper plate, and the two instrument ports were used to seal the chamber, hence the test results also apply to them. An aluminum plate was used instead of the copper plate without influencing the results.
B. A Norgren R43-201-NNLA regulator with an Ashcroft pressure gauge calibrated in house.
C. Tests were performed Juan Carlos Gonzalez.
D. Tests were done in order to obtain a maximum limit for the part being tested. That value was then used to calculate the maximum tolerance in the applicable load configuration. The pressure was raised two 55 psi absolute. It was kept at that level for 20 seconds. The pressure was then lowered to 50 psi absolute and kept that level for 10 minutes. No leakage or rupture occurred.

Name: Juan Carlos Gonzalez

Signature: 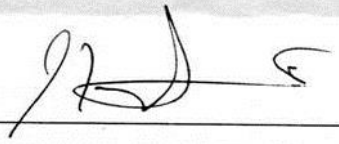

Date: 02/14/2012

Low Pressure Tank Hydrostatic Test Sheet.

The low pressure tank was submitted to a hydrostatic test The manufacturer states that the tank's pressure rating is 50 PSI. Given that, the pressure applied to the tank was 1.5 times the rating spec, (75 PSI).

A. The test was done by filling the tank with water, attaching in to a standard tap water outlet in order to pressurize it.
B. A Norgren R43-201-NNLA regulator with an Ashcroft pressure gauge calibrated in house.
C. Tests were performed Juan Carlos Gonzalez.
D. Tests were done in order to obtain a maximum limit for the part being tested. That value was then used to calculate the maximum tolerance in the applicable load configuration. The pressure was raised two 75 psi absolute. It was kept at that level for 1 minute. No leakage or rupture occurred.

Name: Juan Carlos Gonzalez

Signature: 

Date: 7/29/12